Journal of Climate

Is there an optimal ENSO pattern that enhances large-scale atmospheric processes conducive to tornado outbreaks in the U.S?

--Manuscript Draft--

Manuscript Number:	JCLI-D-12-00128
Full Title:	Is there an optimal ENSO pattern that enhances large-scale atmospheric processes conducive to tornado outbreaks in the U.S?
Article Type:	Article
Corresponding Author:	Sang-Ki Lee, Ph.D. University of Miami Miami, FL UNITED STATES
Corresponding Author's Institution:	University of Miami
First Author:	Sang-Ki Lee, Ph.D.
Order of Authors:	Sang-Ki Lee, Ph.D.
	Robert Atlas, Ph.D.
	David Enfield, Ph.D.
	Chunzai Wang, Ph.D.
	Hailong Liu, Ph.D.
Abstract:	The record-breaking U.S. tornado outbreaks in the spring of 2011 prompt the need to identify long-term climate signals that could potentially provide seasonal predictability for U.S. tornado outbreaks. Here we use both observations and model experiments to show that a positive phase Trans-Niño may be one such climate signal. Among the top ten extreme outbreak years during 1950-2010, seven years including the top three are identified with a strongly positive phase Trans-Niño. The number of intense tornadoes in April - May is nearly doubled during the top ten positive Trans-Niño years from that during ten neutral years. Trans-Niño represents the evolution of tropical Pacific sea surface temperatures (SSTs) during the onset or decay phase of the El Niño-Southern Oscillation. A positive phase Trans-Niño is characterized by colder-than-normal SSTs in the central tropical Pacific and warmer-than-normal SSTs in the eastern tropical Pacific. Modeling experiments suggest that warmer-than-normal SSTs in the eastern tropical Pacific work constructively with colder-than-normal SSTs in the central tropical Pacific to force a strong and persistent teleconnection pattern that increases both the upper-level westerly and lower-level southeasterly over the central and eastern U.S. These anomalous winds advect more cold and dry upper-level air from the high-latitudes and more warm and moist lower-level air from the Gulf of Mexico converging into the east of the Rockies, and also increase both the lower-tropospheric (0 ~ 6 km) and lower-level (0 ~ 1 km) vertical wind shear values therein, thus providing large-scale atmospheric conditions conducive to intense tornado outbreaks over the U.S.

Corresponding author: Sang-Ki Lee
CIMAS, University of Miami and AOML, NOAA, Miami, FL 33149
E-mail) sang-ki.lee@noaa.gov

Dear Dr. Cook,

We have made a further revision of our manuscript based on additional comments from new reviewer #1. As requested by new reviewer #1, a scatter plot of the TNI versus the number of intense tornadoes is added in the revised manuscript (new Figure 3). Additionally, a sentence is added to indicate that the overall correlation between the TNI and tornadic environments is weak. On his/her comment #2, we already performed ranking correlation analysis using Spearman's rho method and found an overall weak correlation between the TNI and the number of intense U.S. tornadoes in our previous revision. We hope that new reviewer #1's major concern is adequately addressed in our newly revised manuscript.

Additionally, Table 5 is now removed to make the manuscript more concise and focused. Some minor editorial changes are done to improve the quality of the manuscript.

Sincerely yours,

Sang-Ki Lee

Page and Color Charge Estimate Form

Click here to download Page and Color Charge Estimate Form: Page_Charge_Estimation_Form.pdf

Review of manuscript: JCLI-D-12-00128

After reading the manuscript carefully, as well as the reviews that were done in a previous version of this paper, I was stunned and dismayed. The authors basically ignored all comments and suggestions done by reviewer 2. I consider that the comments done by reviewer 2 are extremely important, basic to the conclusions of the paper and very relevant and definitely need to be taken into account by the authors in order for this paper to be considered for publication in Journal of Climate. Without taking these important issues into account, I can only recommend the rejection of this paper.

We thank new reviewer #1 for his/her careful review and helpful comments. We would like to appeal to new reviewer #1 that we have no intention to refuse to show additional results suggested by old reviewer #2. We and old reviewer #2 have different opinion about how useful those additional materials may contribute to the manuscript.

Thanks to you and the editor, we are now convinced that adding some of those additional materials could be useful for readers to better understand the overall weak correlation between the TNI and the number of intense tornadoes. On that very point, we performed ranking correlation analysis using Spearman’s rho method as you suggested in your comment #2. We also performed Pearson correlation analysis after removing 1974 as suggested by old reviewer #2. These additional correlation analyses suggest an overall weak correlation between the TNI and the number of intense U.S. tornadoes. These are discussed in the beginning of the section 3 (page 5, line 21 – page 6, line 23). After that, we analyzed further and found that although the overall correlation between the TNI and the number of intense U.S. tornadoes is not strong, extremely active years are frequently linked to a positive phase TNI.

As requested, a scatter plot of the TNI versus the number of intense tornadoes is also added in the revised manuscript (new Figure 3). Additionally, a sentence is added to indicate that the overall correlation between the TNI and tornadic environments is weak.

We hope that new reviewer #1’s major concern is adequately addressed in our revised manuscript.

I would stress the following important issues that need to be done by the authors:

1. Show a scatter plot of TNI and AM tornadoes - this is basic, show the data and how the relationship you are discussing appears in the data. It's not acceptable to refuse to show the data. The arguments based on a discussion Table 2 need be backed up by the complete datasets.

As requested, a scatter plot of TNI and the number of intense U.S. tornadoes in AM is shown below.

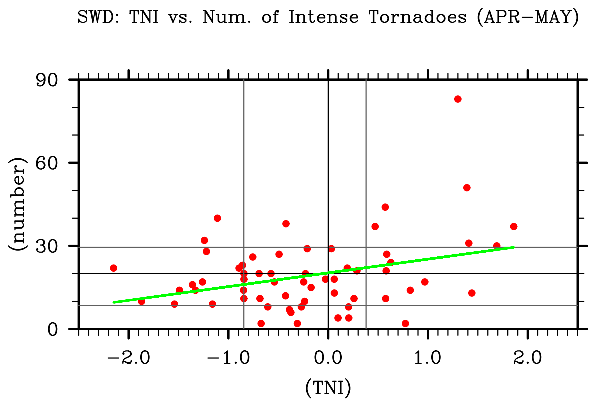

The green line shows the least-squares regression fit with its slope (α = 4.96) exceeding 99% confidence limit (i.e. the null hypothesis that α is not different from 0 is rejected at the two tailed 99% significance level). The vertical lines to the left and right of the zero line show the lower and upper quartiles of the TNI index, respectively. The horizontal lines above and below the mean separate normal activity years from the 10 most active and 10 least active years. This plot basically shows that the TNI and the number of intense tornadoes have an overall weak and positive relationship. This plot also shows that 7 out of the 10 most active years occurred during positive phase TNI years, whereas 10 least active years occurred largely during neutral TNI years, in agreement with Table 1, 2 and 3. This plot is now added as Figure 3 in the revised manuscript.

2. I agree with reviewer #2 that the Pearson correlation is inappropriate here. If the authors want to keep the Pearson correlation in the paper, they need to add other non-parametric measures in the paper: Kendall's tau and Spearman's who. I think it's not acceptable to refuse to show these results and just change the language used for significance in the paper.

As mentioned above, we performed ranking correlation analysis using Spearman's rho method as requested. We also performed Pearson correlation analysis after removing 1974 as suggested by old reviewer #2. These additional correlation analyses suggest an overall weak correlation between the TNI and the number of intense U.S. tornadoes. These are discussed in the beginning of the section 3 (page 5, line 21 – page 6, line 16) of the revised manuscript.

3. Tornadoes time-series F2-F5 vs. F3-F5. I would like to see a comparison of both time-series and a discussion on how the results, i.e. correlations (inclusing Kendall's and Sperman's - see item 2) change if F2-F5 tornadoes are considered. The robustness of the results should be discussed here.

As requested, the Pearson and ranking correlation (Spearman's rho) coefficients of TNI with the number of F0-F5, F1-F5, F2-F3 and F3-F5 tornadoes are shown in the following table.

Fujita-Scales	Pearson	Spearman's rho
F3-F5	**0.33** (**0.29**)	0.16 (**0.25**)
F2-F5	0.22 (0.21)	0.09 (0.15)
F1-F5	0.18 (0.15)	0.09 (0.08)
F0-F5	0.02 (0.05)	0.02 (0.00)

The correlation coefficients generally decrease as weaker tornadoes are included. This result can be interpreted in multiple ways. It may suggest that TNI is associated more with stronger tornadoes than weaker tornadoes. One can also argue that the TNI and U.S tornado activity are not strongly correlated because the results are not consistent when different Fujita scales are used as new reviewer #1 implied here. This result may also reflect that there are more uncertainties in weaker tornadoes counts in the NOAA's severe weather database. Therefore, this result shown in the above table does not necessarily indicate that our results shown in Table 1 are not robust. Since this result can be interpreted in multiple ways and thus confusing, we prefer not to add this result in the revised manuscript.

Additionally, since we have already concluded in the revised manuscript that the overall correlation between the TNI and the number of U.S. tornadoes is weak, we feel that it is not necessary to add more correlation analysis to strengthen that conclusion.

4. Please do show the correlation of TNI with vertical shear and moisture. If your results are significant, the connection should be appear in these results.

The correlation between the TNI and moisture transport is positive, but very weak (r = 0.03). The correlation of the TNI with the lower-level wind shear is also positive and weak (r = 0.11). This result is consistent with our finding that the overall correlation between the TNI and U.S. tornado activity is weak as we discussed in the revised manuscript (page 5, line 21 – page 6, line 16). This point is now added in the revised manuscript (Page 6, line 16): "Similarly, the TNI is only weakly correlated with tornadic environments (not shown)".

Finally, we would like to point out that the Gulf-to-U.S. moisture transport and the lower-level wind shear east of the Rockies are significantly (at the 90% confidence level) increased during the ten positive TNI years (Figure 5b and c).

Is there an optimal ENSO pattern that enhances large-scale atmospheric processes conducive to tornado outbreaks in the U.S?

Sang-Ki Lee[1,2], Robert Atlas[2], David Enfield[1,2], Chunzai Wang[2], and Hailong Liu[1,2]

[1]Cooperative Institute for Marine and Atmospheric Studies, University of Miami, Miami, Florida, USA

[2]Atlantic Oceanographic and Meteorological Laboratory, NOAA, Miami Florida, USA

USA

June 2012

Corresponding author address: Dr. Sang-Ki Lee, NOAA/AOML, 4301 Rickenbacker Causeway, Miami, FL 33149, USA. E-mail: Sang-Ki.Lee@noaa.gov.

Abstract

The record-breaking U.S. tornado outbreaks in the spring of 2011 prompt the need to identify long-term climate signals that could potentially provide seasonal predictability for U.S. tornado outbreaks. Here we use both observations and model experiments to show that a positive phase Trans-Niño may be one such climate signal. Among the top ten extreme outbreak years during 1950-2010, seven years including the top three are identified with a strongly positive phase Trans-Niño. The number of intense tornadoes in April - May is nearly doubled during the top ten positive Trans-Niño years from that during ten neutral years. Trans-Niño represents the evolution of tropical Pacific sea surface temperatures (SSTs) during the onset or decay phase of the El Niño-Southern Oscillation. A positive phase Trans-Niño is characterized by colder-than-normal SSTs in the central tropical Pacific and warmer-than-normal SSTs in the eastern tropical Pacific. Modeling experiments suggest that warmer-than-normal SSTs in the eastern tropical Pacific work constructively with colder-than-normal SSTs in the central tropical Pacific to force a strong and persistent teleconnection pattern that increases both the upper-level westerly and lower-level southeasterly over the central and eastern U.S. These anomalous winds advect more cold and dry upper-level air from the high-latitudes and more warm and moist lower-level air from the Gulf of Mexico converging into the east of the Rockies, and also increase both the lower-tropospheric (0 ~ 6 km) and lower-level (0 ~ 1 km) vertical wind shear values therein, thus providing large-scale atmospheric conditions conducive to intense tornado outbreaks over the U.S.

1. Introduction

In April and May of 2011, a record breaking 1,084 tornadoes and 538 tornado-related fatalities were confirmed in the U.S., making 2011 one of the deadliest tornado years in U.S. history [http://www.spc.noaa.gov/climo/online/monthly/newm.html#2011]. Questions were raised almost immediately as to whether the series of extreme tornado outbreaks in 2011 could be linked to long-term climate variability. The severe weather database (SWD) from the National Oceanic and Atmospheric Administration indicates that the number of total U.S. tornadoes (i.e., from F0 to F5 in the Fujita-Pearson scale) during the most active tornado months of April and May (AM) has been steadily increasing since 1950 (Figure 1). However, due to numerous known deficiencies in the SWD, including improvements in tornado detection technology, increased eyewitness reports due to population increase, and changes in damage survey procedures over time, one must be cautious in attributing this secular increase in the number of U.S. tornadoes to a specific long-term climate signal (Brooks and Doswell 2001; Verbout et al. 2006). In this study, only the intense U.S. tornadoes (i.e., from F3 to F5 in the Fujita-Pearson scale) are selected and used since intense and long-track tornadoes are less likely to be affected by, although they are not completely free from, the known issues in the tornado database.

In the U.S. east of the Rocky Mountains, cold and dry upper-level air from the high latitudes often converges with warm and moist lower-level air coming from the Gulf of Mexico (GoM). Due to this so-called large-scale differential advection, i.e., any vertical variation of the horizontal advection of heat and moisture that decreases the vertical stability of the air column (Whitney and Miller 1956), a conditionally unstable atmosphere with high convective available potential energy is formed. The lower-tropospheric (0 ~ 6 km) vertical wind shear associated with the upper-level westerly and lower-level southeasterly winds (i.e., wind speed increasing and/or wind direction changing with height) provides the rotation with respect to a horizontal axis. The axis of this horizontal vortex tube can be tilted to the vertical by updrafts and downdrafts to form an intense rotating thunderstorm known as a supercell, which is the storm type most apt to spawn intense tornadoes (Lemon and Doswell 1979; Doswell and Bosart 2001). Increased low-level (0 ~ 1 km) vertical wind shear is an additional atmospheric condition that distinguishes tornadic supercells from non-tornadic supercells. Consistently, the moisture transport from the GoM to the U.S. and both the lower-tropospheric and lower-level vertical wind shear values in the central and eastern U.S. are positively correlated with the number of intense U.S. tornadoes in AM (Table 1).

The Pacific - North American (PNA) pattern in boreal winter and spring is linked to the large-scale differential advection and the lower-tropospheric vertical wind shear in the central and eastern U.S (Horel and Wallace 1981; Walalce and Gutzler 1981; Barnston and Livezey 1987). During a negative phase of the PNA, an anomalous upper-level cyclone is formed over North America that shifts the jet stream (and also the mid-latitude storm tracks) northward, thus advecting more cold and dry upper-level air to the central and eastern U.S., and an anomalous anticyclone is formed over the southeastern seaboard that increases the southwesterly wind from the GoM to the U.S., thus enhancing the Gulf-to-U.S. moisture transport. The upper-level cyclone also contributes to the development of steep lapse rates and removal of convective inhibition in the region of strong rising motion downstream from the cyclone (due to differential vorticity advection) and thus sets up a favorable environment for tornadogenesis (e.g., Doswell and Bosart 2001). Additionally, the lower-tropospheric vertical wind shear is increased over the central and eastern U.S. during a negative phase of the PNA due to the increased upper-level westerly and lower-level southeasterly flow.

Although the PNA is a naturally occurring atmospheric phenomenon driven by intrinsic variability of the atmosphere, a La Niña in the tropical Pacific can project onto a negative phase PNA pattern (Lau and Lim 1984; Straus and Shukla 2002). In addition, since the Gulf-to-U.S. moisture transport can be enhanced with a warmer GoM, the sea surface temperature (SST) anomaly in the GoM can also affect U.S. tornado activity. During the decay phase of La Niña in spring, the GoM is typically warmer than usual (Alexander and Scott 2002). Therefore, the Gulf-to-U.S. moisture transport could be increased during the decay phase of La Niña in spring due to the increased SSTs in the GoM and the strengthening of the southwesterly wind from the GoM to the U.S. Nevertheless, the connectivity between the El Niño-Southern Oscillation (ENSO) and U.S. tornado activity in AM is quite weak (Table 1) as reported in earlier studies (Marzaban and Schaeffer 2001; Cook and Schafer 2008). Currently, seasonal forecast skill for intense U.S. tornado outbreaks, such as occurred in 2011, has not been demonstrated.

Interestingly, among the long-term climate patterns considered in Table 1, the number of U.S. tornadoes in AM is more strongly correlated with the Trans-Niño (TNI) than any other climate pattern. The TNI, which is defined as the difference in normalized SST anomalies between the Niño-1+2 (10S° - 0°; 90°W - 80°W) and Niño-4 (5°N - 5°S; 160°E - 150°W) regions, represents the evolution of ENSO in the months leading up to the event and the subsequent evolution with opposite sign after the event (Trenberth and Stepaniak 2001). Given that AM is typically characterized with the onset or decay phase of ENSO events, it is more likely that the tropical Pacific SST patterns in AM associated with ENSO are better represented by the TNI index than the conventional ENSO indices such as Niño-3.4 (5°N - 5°S; 170°W - 120°W) or Niño-3 (5°N - 5°S; 150°W-90°W). Nevertheless, it is not clear why U.S. tornado activity in AM is more strongly correlated with the TNI index than with other ENSO indices.

This is the central question that we explore in the following sections by using both observations and an atmospheric general circulation model (AGCM).

2. U.S. tornado index

Since intense and long-track tornadoes are much more likely to be detected and reported even before a national network of Doppler radar was build in the 1990s, only the intense U.S. tornadoes in AM during 1950-2010 from the SWD are selected and used in this study. The number of intense U.S. tornadoes is used, after detrending, as the primary diagnostic index (Figure 2b). Another tornado metric used in this study is the intense U.S. tornado-days (Figure 2c and d), which is obtained by counting the number of days in which more than a threshold number of intense tornadoes occurred (see Verbout et al. 2006). The threshold number selected in this case is three and above, which roughly represents the upper quartile in the number of intense U.S. tornadoes in a given day of AM during 1950-2010. In general, the tornado count index is sensitive to big tornado outbreak days, such as April 3, 1974 during which 60 intense tornadoes occurred over the U.S. The tornado-days index, on the other hand, puts little weight on big tornado days. Since these two tornado indices are complementary to each other, it is beneficial to use both of these indices. The two tornado indices are further detrended by using a simple least squares linear regression.

3. Observed relationship between TNI and extreme U.S. tornado outbreaks

Table 1 shows that the TNI is significantly correlated with the number of intense tornadoes in AM. However, it is noted that the historical time series for the number of intense tornadoes is characterized by intense tornado outbreak years, such as 1974, 1965 and 1957, embedded amongst much weaker amplitude fluctuations (Figure 2a and b). Therefore, the common practice of applying linear correlation (i.e., Pearson correlation) in this case is limited by the skewness (i.e., non-Gaussian distribution) in the tornado time series. This issue with the tornado time series can be seen more clearly in the scatter plot of the TNI versus the number of intense tornadoes in AM (Figure 3). A simple way to remedy this data issue is to remove the most extreme year of 1974 and repeat the correlation test. In that case, the linear correlation between the TNI and the number of intense tornadoes falls to 0.25, which is barely significant at the 95% significance level based on student's t test. Perhaps, a more formal alternative is to use ranking (or nonparametric) correlation methods, such as Kendall's tau and Spearman's rho, which are not sensitive to extreme years such as 1974. Ranking correlations basically replace the number of tornadoes in each year to its ranking among the 61 years time series. Therefore, 1974 and 1965 will be given the ranking of 1 and 2, respectively. Spearman's rho method is applied to find that the ranking correlation between the TNI and the number of intense tornado (intense tornado-days) falls to 0.16 (0.24), which is below (barely significant at) the 95% significance level, suggesting that the overall correlation between the TNI and the number of intense tornadoes is not strong. Similarly, the TNI is only weakly correlated with tornadic environments (not shown).

However, it is important to note that the ranking correlation gives less weight to extreme outbreak years such as 1974, 1965 and 1957 and more weight to weak amplitude years, whereas the linear correlation is very sensitive to extreme years. What this means is that although the overall correlation between the TNI and the number of intense tornadoes is not strong, the TNI may be associated with extreme outbreak years (see Figure 3). Since the majority of tornado-related fatalities occur during those extreme outbreak years, here we focus our attention to those extreme years and associated large-scale atmospheric processes. Therefore, we first ranked the years from 1950 to 2010 (61 years in total) based on the number of intense U.S. tornadoes in AM. The top ten extreme U.S. tornado outbreak years are listed in Table 2. Note that if the tornado ranking is redone based on the intense U.S tornado-days in AM, 1998 in the top ten list is replaced by 1960, but other top nine years remain in the top ten (not shown).

The top ten extreme tornado outbreak years are characterized by an anomalous upper-level cyclone over North America (Figure 4a), increased Gulf-to-U.S. moisture transport (Figure 4b), increased lower-tropospheric (not shown) and lower-level vertical wind shear values over the east of the Rockies (Figure 4c), whereas the bottom ten years are associated with an anomalous upper-level anticyclone over North America (Figure 4d), decreased Gulf-to-U.S. moisture transport (Figure 4e) and decreased lower-tropospheric (not shown) and lower-level vertical wind shear values over the central and eastern U.S (Figure 4f). It is worthwhile to point out that all the composite maps and model results shown in this study should be understood in a long-term averaged sense. For instance, the anomalous upper-level cyclone over North America shown in Figure 4a is a long-term average over many days during which a series of cyclones as well as anticyclones may have passed over the area.

As in the top ten extreme tornado outbreak years, the top ten positive TNI (i.e., normalized SST anomalies are larger in the Niño-1+2 than in Niño-4 region) years are also characterized by an anomalous upper-level cyclone over North America (Figure 5a), increased Gulf-to-U.S. moisture transport (Figure 5b) and increased lower-tropospheric (not shown) and lower-level vertical wind shear values over the east of the Rockies (Figure 5c). Due to these large-scale atmospheric conditions, the number of intense U.S. tornadoes in AM during the top ten positive TNI years is nearly doubled from that during ten neutral TNI years (Figure 6a and b). Consistent with these findings, among the top ten extreme tornado outbreak years, seven years including the top three are identified with a strongly positive phase (i.e., within the upper quartile) TNI as shown in Table 2 (also see Figure 3). Five out of those seven years are characterized by a La Niña transitioning to a different phase or persisting beyond AM (1957, 1965, 1974, 1999, and 2008) and the other two with an El Niño transitioning to either a La Nina or neutral phase (1983 and 1998). The composite SST anomalies for those five positive phase TNI years transitioning from a La Niña are characterized by colder than normal SSTs in the central tropical Pacific (CP) and warmer than normal SSTs in the eastern tropical Pacific (EP) (Figure 7a) as in the composite SST anomalies for the top ten positive TNI years (Figure 7b). If the top ten extreme tornado outbreak years are averaged together, the composite SST anomalies are still characterized by a positive phase TNI (i.e., normalized SST anomalies are larger in the Niño-1+2 than in Niño-4 region), although the colder than normal SST anomalies in CP are nearly canceled out (Figure 7c).

In the bottom ten years, on the other hand, only one year is identified with a strongly positive phase TNI, and the other nine years are with a neutral phase TNI (i.e., between the lower and upper quartiles) as shown in Table 3 (also see Figure 3). This result suggests that a negative phase of the TNI does not decrease the number of intense U.S. tornadoes in AM, and thus partly explains why the overall correlation between the TNI and the number of intense U.S. tornadoes in AM is not high. Consistently, the number of intense U.S. tornadoes in AM during the top ten negative phase TNI years is not much changed from that during ten neutral phase TNI years (Figure 6b and c). Interestingly, four years among the bottom ten years are identified with a La Niña transitioning to a different phase or persisting beyond AM (1950, 1951, 1955 and 2001), and four are identified with an El Niño transitioning to a different phase or persisting beyond AM (1958, 1987, 1988 and 1992). The composite SST anomaly pattern for the four years of the bottom ten years with a La Niña transitioning is that of a typical La Niña with the SST anomalies in the Niño-4 and Niño-1+2 being both strongly negative (i.e., neutral phase TNI) (Figure 8a). Similarly, the composite SST anomaly pattern for the four years in the bottom ten years with an El Niño transitioning is that of a typical El Niño with the SST anomalies in the Niño-4 and Niño-1+2 being both strongly positive (i.e., neutral phase TNI) (Figure 8b).

In summary, observations seem to indicate that a positive phase of the TNI (i.e., normalized SST anomalies are larger in the Niño-1+2 than in Niño-4 region) is linked to extreme U.S. tornado outbreaks in AM, whereas either La Niñas and El Niños with a neutral phase TNI (i.e., the SST anomalies in the Niño-1+2 region are as strong and the same sign as the SST anomalies in the Niño-4) are not linked to extreme U.S. tornado outbreaks in AM.

4. Model experiments

To explore the potential link between the tropical Pacific SST anomaly patterns, identified in the previous section (Figure 7 and 8), and the number of intense U.S. tornadoes in AM, a series of AGCM experiments are performed by using version 3.1 of the NCAR community atmospheric model coupled to a slab mixed layer ocean model (CAM3). The model is a global spectral model with a triangular spectral truncation of the spherical harmonics at zonal wave number 42. It is vertically divided into 26 hybrid sigma-pressure layers. Model experiments are performed by prescribing various composite evolutions of SSTs in the tropical Pacific region (15°S–15°N; 120°E-coast of the Americas) while predicting the SSTs outside the tropical Pacific using the slab ocean model. To prevent discontinuity of SST around the edges of the forcing region, the model SSTs of three grid points centered at the boundary are determined by combining the simulated and prescribed SSTs. Each ensemble consists of ten model integrations that are initialized with slightly different conditions to represent intrinsic atmospheric variability. The same methodology was previously used for studying ENSO teleconnection to the tropical North Atlantic region (Lee et al. 2008; Lee et al. 2010).

Six sets of ensemble runs are performed (Table 4). In the first experiment (EXP_CLM), the SSTs in the tropical Pacific region are prescribed with climatological SSTs. In the second experiment (EXP_TNI), the composite SSTs of the positive phase TNI years identified among the ten most active U.S. tornado years are prescribed in the tropical Pacific region. Note that only the five positive TNI years transitioning from a La Niña are considered in this case (Figure 7a). Two experiments similar to EXP_TNI are carried out by prescribing the SSTs in the tropical Pacific region with the composite SSTs of the top ten positive TNI years (Figure 7b) for EXP_TN1, and the top ten most extreme tornado years (Figure 7c) for EXP_TN2. In the next two experiments, the SSTs in the tropical Pacific region are prescribed with the composite SSTs of the four years in the bottom ten years with a La Niña transitioning (Figure 8a) for EXP_LAN, and the four years in the bottom ten years with an El Niño transitioning (Figure 8b) for EXP_ELN.

5. Simulated impact of TNI on tornadic environments

In EXP_TNI (Figure 9), an anomalous upper-level cyclone is formed over North America that shifts the jet stream northward, thus advecting more cold and dry upper-level air to the central and eastern U.S. The Gulf-to-U.S. moisture transport and the lower-tropospheric (not shown) and lower-level vertical wind shear values are increased over the central and eastern U.S. All of these are large-scale atmospheric conditions conducive to intense tornado outbreaks over the U.S. and they are also well reproduced in both EXP_TN1 and EXP_TN2 (Figure 10).

In EXP_ELN (Figure 11d, e and f), on the other hand, the Gulf-to-U.S. moisture transport is neither increased nor decreased. A weak anomalous upper-level anticyclone is formed (in a long-term and ensemble averaged sense) over North America, and the lower-tropospheric (not shown) and lower-level vertical wind shear values are slightly decreased over the central and eastern U.S. In EXP_LAN (Figure 11a, b and c), a relatively weak anomalous upper-level cyclone is formed over North America, and thus the lower-tropospheric (not shown) and lower-level vertical wind shear values are increased in the central and eastern U.S. However, the Gulf-to-U.S. moisture transport is not increased.

In summary, these model results support the hypothesis that a positive phase of the TNI with colder than normal SSTs in CP and warmer than normal SSTs in EP enhances the large-scale differential advection in the central and eastern U.S. and increases the lower-tropospheric and lower-level vertical wind shear values therein, thus providing large-scale atmospheric conditions conducive to intense tornado outbreaks over the U.S. However, the model results do not show favorable large-scale atmospheric conditions in the central and eastern U.S. under La Niña and El Niño conditions as long as the SST anomalies in EP are as strong and the same sign as the SST anomalies in CP (i.e., neutral phase TNI), consistent with the observations.

6. CP- versus EP-forced teleconnection

The model results strongly suggest that colder than normal SSTs in CP and warmer than normal SSTs in EP may have a constructive influence on the teleconnection pattern that strengthens the large-scale differential advection and lower-tropospheric and lower-level vertical wind shear values over the central and eastern U.S. To better understand how the real atmosphere with moist diabatic processes responds to colder than normal SSTs in CP and warmer than normal SSTs in EP, two sets of additional model experiments (EXP_CPC and EXP_EPW) are performed (Table 4). These two experiments are basically identical to EXP_TNI except that the composite SSTs of the positive phase TNI years are prescribed only in the western and central tropical Pacific region (15°S–15°N; 120°E - 110°W) for EXP_CPC and only in the eastern tropical Pacific region (15°S–15°N; 110°W-coast of the Americas) for EXP_EPW. Note that climatological SSTs are prescribed in the eastern Pacific region (15°S–15°N; 110°W-coast of the Americas) for EXP_CPC and in the western and central tropical Pacific region (15°S–15°N; 120°E - 110°W) for EXP_EPW.

In EXP_CPC (Figure 12a, b and c), the teleconnection pattern emanating from the tropical Pacific consists of an anticyclone over the Aleutian Low in the North Pacific, a cyclone over North America, and an anticyclone over the southeastern U.S. extending to meso-Americas, consistent with a negative phase PNA-like pattern (Figure 12a). As expected from the anomalous anticyclonic circulation over the southeastern U.S. and meso-America, the Gulf-to-U.S. moisture transport is increased in EXP_CPC (Figure 12b). The lower-tropospheric (not shown) and lower-level vertical wind shear values are also increased over the central and eastern U.S. due to the strengthening of the upper-level westerly and lower-level southeasterly winds (Figure 12c).

Surprisingly, the Rossby wave train forced by warmer than normal SSTs in EP (EXP_EPW) is very similar to that in EXP_CPC (Figure 12d). Consistently, the Gulf-to-U.S. moisture transport and the lower-tropospheric (not shown) and lower-level vertical wind shear values over the central and eastern U.S. are also increased in EXP_EPW (Figure 12e and f) as in EXP_CPC and EXP_TNI. A question arises as to why the teleconnection pattern forced by warmer than normal SSTs in EP is virtually the same as that forced by colder than normal SSTs in CP. It appears that the Rossby wave train in EXP_EPW is not directly forced from EP. In EXP_EPW, convection is increased locally in EP, but it is decreased in CP as in EXP_CPC (Figure 13c). This suggests that increased convection in EP associated with the increased local SSTs suppresses convection in CP and that in turn forces a negative phase PNA-like pattern. Therefore, these model results confirm that colder than normal SSTs in CP and warmer than normal SSTs in EP do have constructive influence on the teleconnection pattern that strengthens the large-scale differential advection and lower-tropospheric and lower-level vertical wind shear values over the central and eastern U.S. The model results also suggest that colder than normal SSTs in CP with neutral SST anomalies in EP or warmer than normal SSTs in EP with neutral SST anomalies in CP can also strengthen the large-scale differential advection and lower-tropospheric and lower-level vertical wind shear values over the east of the Rockies.

An apparently important question is why warmer than normal SSTs in EP does not directly excite a Rossby wave train to the high-latitudes. As shown in earlier theoretical studies, the background vertical wind shear is one of the two critical factors required for tropical heating to radiate barotropic teleconnections to the high-latitudes (e.g., Kasahara and da Silva Dias 1986; Wang and Xie 1996; Lee et al. 2009). In both observations and EXP_CLM, the background vertical wind shear between 200 and 850 hPa in AM is largest in the central tropical North Pacific and smallest in EP and the western tropical Pacific (WP), providing a potential explanation as to why the Rossby wave train in EXP_EPW is not directly forced in EP (Figure 14).

Another related and important question is how increased convection in EP associated with the increased local SSTs suppresses convection in CP remotely. Although answering this question requires a more extensive study, one potential explanation is that the warmer than normal SSTs in EP induces a global average warming of the tropical troposphere via a fast tropical teleconnection mechanism (e.g., Chiang and Sobel 2002), and thus increases atmospheric static stability and decreases convection over CP and other tropical regions of normal SSTs. A similar argument was previously used in Lee et al. (2011) to explain reduced deep convection in the tropical Atlantic in response to warmer than normal SSTs in the tropical Pacific. Another similar argument, but in a different context, is the "upped-ante mechanism", which is often used to explain anomalous descent motions neighboring warm SST anomalies in the eastern and central Pacific Ocean during El Niño (Su and Neelin 2002; Neelin et al. 2003).

7. Implications for a seasonal outlook for extreme U.S. tornado outbreaks

The conclusion so far is that a positive phase of the TNI, characterized by colder than normal SSTs in CP and warmer than normal SSTs in EP, strengthens the large-scale differential advection and lower-tropospheric and lower-level vertical wind shear values in the central and eastern U.S., and thus provides favorable large-scale atmospheric conditions for major tornado outbreaks over the U.S. In this sense, a positive phase of the TNI may be an optimal ENSO pattern that increases the chance for major U.S. tornado outbreaks. However, the TNI explains only up to 10% of the total variance in the number of intense U.S. tornadoes in AM. This suggests that intrinsic variability in the atmosphere may overwhelm the positive phase TNI-teleconnection pattern over North America as discussed in earlier studies for El Niño-teleconnection patterns in the Pacific–North American region (e.g., Hoerling and Kumar 1997). In other words, the predictability of U.S. tornado activity, which can be defined as a ratio of the climate signal (the TNI index in this case) relative to the climate noise, is low.

Nevertheless, seven of the ten most extreme tornado outbreak years during 1950-2010 including the top three years are characterized by a strongly positive phase of the TNI (Table 2), and the number of intense U.S. tornadoes in AM during the top ten positive phase TNI years is nearly doubled from that during ten neutral phase TNI years (Figure 6). A practical implication of these results is that a seasonal outlook for extreme U.S. tornado outbreaks may be achievable if a seasonal forecasting system has significant skill in predicating the TNI and associated teleconnections to the U.S. Obviously, before we can achieve such a goal, there remain many crucial scientific questions to be addressed to refine the predictive skill provided by the TNI and to explore other long-term climate signals that can provide additional predictability in seasonal and longer time scales.

8. Historical U.S. tornado outbreak years

In terms of annual tornado-related death toll, 2011 was the 4th deadliest tornado year in the U.S. history after 1925, 1936 and 1917 (Doswell et al. 2012). 1974 was the 14th, but it was the year in which the largest number of intense tornadoes occurred (Table 2). A positive phase of the TNI prevailed during AM of 2011, 1974 and 1925 with colder than normal SSTs in CP and warmer than normal SSTs in EP (Figure 15). A positive phase TNI also occurred during AM of the other two historical outbreak years (not shown). In particular, the TNI during AM of 1917 is marked as the strongest TNI during the period of 1854 - 2011. An important question is whether the series of extreme U.S. tornado outbreaks during AM of 2011 and the other historical U.S. tornado outbreak years can be attributed to the positive phase TNI.

During AM of 2011, an anomalous upper-level cyclone was formed over the northern U.S. and southern Canada (Figure 16a), the Gulf-to-US moisture was greatly increased (Figure 16b), and the lower-tropospheric (not shown) and lower-level vertical wind shear values were increased over the east of the Rockies (Figure 16c). All of these atmospheric conditions, clearly indicating the coherent teleconnection response to a positive phase TNI, also prevailed in AM of 1974 (Figure 16d, e and f).

To confirm this finding, a set of additional model experiments (EXP_011) is performed by prescribing the SSTs for 2010 - 2011 in the tropical Pacific region while predicting the SSTs outside the tropical Pacific using the slab ocean model (Table 4). The model results are consistent with the observations, although the anomalous Gulf-to-US moisture transport is weaker in the model experiment (not shown). Thus, it is highly likely that the 2011 positive phase TNI event did contribute to the U.S. tornado outbreak in AM of 2011 by enhancing the differential advection and lower-tropospheric and lower-level vertical wind shear values in the central and eastern U.S. A distinctive feature in the 2011 TNI event is warmer than normal SSTs in WP (Figure 15a). A further experiment (EXP_WPW) suggest that the warmer than normal SSTs in WP indirectly suppress convection in CP, and thus work constructively with the colder than normal SSTs in CP to force a strong and persistent negative phase PNA-like pattern (not shown).

9. Discussions

Tornadogenesis is basically a mesoscale problem that requires overlap of very specific and highly localized atmospheric conditions. Therefore, it is not expected to be adequately captured by large-scale and long-term averaged atmospheric processes. In this study, we simply argue that such overlap of the specific conditions for tornadogenesis may occur more frequently on average during a positive phase of the TNI. In addition to the large-scale atmospheric conditions explored in this study, there are other specific atmospheric conditions for tornadogenesis such as lifting condensation level height and convective inhibition. Their associations with the TNI need to be explored in future studies.

It appears that a positive phase of the TNI is associated more with intense tornado activity over the Ohio River Valley region, and less with intense tornado activity over the Great Plains (Figure 6). Recent studies reported that springtime tornado activity over the Ohio River Valley region is closely linked to the preferred modes of variability in North American low-level jet (NALLJ) and their shifts in longer time scales (Muñoz and Enfield 2011; Weaver et al. 2012). Future studies need to address the potential linkage among the TNI, the modes of variability in NALLJ and regional U.S. tornado activity.

One of the caveats in this study, as in any tornado related climate research, is an artificial inhomogeneity in the tornado database. Eyewitness reports are important sources for tornado count, which can be affected by population growth and migration. Additionally, tornado rating is largely based on structural damage - wind speed relationship, which can change with time and case-by-case because every particular tornado - structure interaction is different in detail. For these and other reasons, the historical time series of the tornado database cannot be completely objective or consistent over time (Doswell et al. 2009). In this study, only the intense U.S. tornadoes (F3 - F5) are selected and used since intense and long-track tornadoes are less likely to be affected by, although they are not completely free from, such issues in the tornado database. An alternative approach is to develop and use a proxy tornado database, which can be derived from tornadic environmental conditions in atmospheric reanalysis products. Results from recent studies that used such an approach were very promising (Brooks et al. 2003; Tippett et al. 2012).

Acknowledgments. We would like to thank Harold Brooks, Charles Doswell, Brian Mapes, Gregory Carbin, Kerry Cook and five anonymous reviewers for their thoughtful comments and suggestions. This study was motivated and benefited from interactions with scientists at NOAA NSSL, ESRL, GFDL, CPC, NCDC and AOML. In particular, we wish to thank Wayne Higgins, Tom Karl and Marty Hoerling for initiating and leading discussions that motivated this study. This work was supported by grants from the National Oceanic and Atmospheric Administration's Climate Program Office and by grants from the National Science Foundation.

REFERNCES

Alexander, M., and J. Scott, 2002: The influence of ENSO on air-sea interaction in the Atlantic. *Geophys. Res. Lett.*, **29**, 1701, doi:10.1029/2001GL014347.

Barnston A. G., and R. E. Livezey, 1987: Classification, seasonality, and persistence of low-frequency atmospheric circulation patterns. Mon. Weather Rev., **115**, 1083–1126.

Brooks, H. E., C. A. Doswell III, 2001: Some aspects of the international climatology of tornadoes by damage classification. *Atmos. Res*. **56**, 191– 201.

Brooks, H. E., J. W. Lee, and J. P. Cravenc, 2003: The spatial distribution of severe thunderstorm and tornado environments from global reanalysis data, *Atmos. Res*., **67-68**, 73-94.

Cook, A. R., J. T. Schaefer, 2008: The relation of El Niño–Southern Oscillation (ENSO) to winter tornado outbreaks, *Mon. Wea. Rev*., **136**, 3121–3137.

Doswell III, C. A., L. F. Bosart, 2001: Extratropical synoptic-scale processes and severe convection. Severe Convection Storms. *Meteor. Monogr*. **28**, Amer. Meteor. Soc. 27-69.

Doswell III, C. A., H. E. Brooks, and N. Dotzek, 2009: On the implementation of the Enhanced Fujita Scale in the USA. *Atmos. Res*., **93**, 554-563, doi:10.1016/j.atmosres.2008.11.003.

Doswell III, C. A., G. W. Carbin, and H. E. Brooks, 2012: The tornadoes of spring 2011 in the USA: an historical perspective. *Wea*., **67**, 88-94.

Hoerling, M. P, and A. Kumar, 1997: Why do North American climate anomalies differ from one El Niño event to another?, *Geophys. Res. Lett*., **24**, 1059-1062.

Horel, J. D., and J. M. Wallace, 1981: Planetary-scale atmospheric phenomena associated with the Southern Oscillation. *Mon. Wea. Rev.* **109**, 813–829.

Kasahara, A., and P. L. da Silva Dias, 1986: Response of planetary waves to stationary tropical heating in a global atmosphere with meridional and vertical shear. *J. Atmos. Sci*., **43**, 1893–1911.

Lau, K.-M., and H. Lim, 1984: On the dynamics of equatorial forcing of climate teleconnections. *J. Atmos. Sci*., **41**, 161–176.

Lee, S.-K., D. B. Enfield, and C. Wang, 2008: Why do some El Ninos have no impact on tropical North Atlantic SST? *Geophys. Res. Lett.*, **35**, L16705, doi:10.1029/2008GL034734.

Lee, S.-K., C. Wang, and B. E. Mapes, 2009: A simple atmospheric model of the local and teleconnection responses to tropical heating anomalies. *J. Clim*., **22**, 272-284.

Lee, S.-K., C. Wang, and D. B. Enfield, 2010: On the impact of central Pacific warming events on Atlantic tropical storm activity. *Geophys. Res. Lett*., **37**, L17702, doi:10.1029/2010GL044459.

Lee, S.-K., D. B. Enfield, and C. Wang, 2011: Future impact of differential inter-basin ocean warming on Atlantic hurricanes. *J. Clim.*, **24**, 1264-1275.

Lemon, L. R., and C. A. Doswell III, 1979: Severe thunderstorm evolution and mesocyclone structure as related to tornadogenesis. *Mon. Wea. Rev.* **107**, 1184–1197.

Marzban, C., and J. Schaefer, 2001: The correlation between U.S. tornados and Pacific sea surface temperature, *Mon. Wea. Rev.*, **129**, 884-895.

Muñoz, E., and D. Enfield, 2011: The boreal spring variability of the Intra-Americas low-level jet and its relation with precipitation and tornadoes in the eastern United States, *Clim. Dyn.*, **36**, 247–259, doi:10.1007/s00382-009-0688-3.

Neelin, J. D., C. Chou, and H. Su, 2003: Tropical drought regions in global warming and El Nino teleconnections. *Geophys. Res. Lett.*, **30**, doi:10.1029/2003GLO018625.

Straus, D. M., J. Shukla, 2002: Does ENSO force the PNA?, *J. Clim.*, **15**, 2340–2358.

Su, H., and J. D. Neelin, 2002: Teleconnection mechanisms for tropical Pacific descent anomalies during El Niño. *J. Atmos. Sci.*, **59**, 2694-2712.

Tippett, M. K., A. H. Sobel, and S. J. Camargo, 2012: Association of U.S. tornado occurrence with monthly environmental parameters, *Geophys. Res. Lett.*, **39**, L02801, doi:10.1029/2011GL050368.

Trenberth, K. E., and D. P. Stepaniak, 2001: Indices of El Niño evolution, *J. Clim.*, **14**, 1697–1701.

Verbout, S. M., H. E. Brooks, L. M. Leslie, and D. M. Schultz, 2006: Evolution of the U.S. tornado database: 1954-2003. *Wea. Forecasting* **21**, 86-93.

Wallace, J. M., and D. S. Gutzler, 1981: Teleconnections in the geopotential height field during the Northern Hemisphere winter. *Mon. Wea. Rev*. **109**, 784–804.

Wang, B., and X. Xie, 1996: Low-frequency equatorial waves in vertically sheared zonal flow. Part I: Stable waves. *J. Atmos. Sci.*, **53**, 449–467.

Weaver, S. J., S. Baxter, and A. Kumar, 2012: Climatic role of North American low-level jets on U.S. regional tornado activity. *J. Clim*., in-press.

Whitney Jr., L. F., and J. E. Miller, 1956: Destabilization by differential advection in the tornado situation 8 June 1953. *Bull. Amer. Meteor. Soc*. **37**, 224–229.

Table 1. Correlation coefficients of various long-term climate patterns in December-February (DJF), February-April (FMA), and April and May (AM) with the number of intense tornadoes in AM during 1950-2010. The values in parenthesis are those with the intense U.S. tornado-days in AM during 1950-2010. All indices including the tornado index are detrended using a simple least squares linear regression. Correlation coefficients above the 95% significance based on student's t test are in bold. The SWD, ERSST3, and NCEP-NCAR reanalysis are used to obtain the long-term climate indices used in this table[a].

Index	DJF	FMA	AM
Gulf-to-U.S. moisture transport	0.12 (0.09)	0.22 (0.10)	**0.44 (0.34)**
Lower-Tropospheric (500 – 1000 hPa) wind shear	0.03 (0.04)	0.16 (0.14)	**0.26** (0.23)
Lower-Level (850 – 1000 hPa) wind shear	0.12 (0.09)	0.20 (0.12)	**0.44 (0.35)**
GoM SST	0.15 (0.15)	0.21 (0.16)	0.20 (0.19)
Niño-4	-0.22 (-0.19)	-0.20 (-0.18)	-0.19 (-0.18)
Niño-3.4	-0.13 (-0.11)	-0.13 (-0.12)	-0.11 (-0.11)
Niño-1+2	0.02 (0.03)	0.11 (0.11)	0.15 (0.13)
TNI	**0.28 (0.26)**	**0.29 (0.28)**	**0.33 (0.29)**
PNA	-0.05 (-0.02)	-0.10 (-0.06)	-0.20 (-0.16)
PDO	-0.12 (-0.09)	-0.10 (-0.11)	-0.14 (-0.20)
NAO	-0.01 (-0.07)	-0.10 (-0.14)	-0.18 (-0.18)

[a]The Gulf-to-U.S. moisture transport is obtained by averaging the vertically integrated moisture transport in the region of 30°N - 40°N and 100°W - 80°W. The wind shear terms are also averaged over the same region. The North Atlantic Oscillation (NAO) index and the Pacific - North American (PNA) pattern are defined as the first and second leading modes of Rotated Empirical Orthogonal Function analysis of monthly mean geopotential height at 500 hPa, respectively. The Pacific Decadal Oscillation (PDO) is the leading principal component of monthly SST anomalies in the North Pacific Ocean north of 20°N.

Table 2. The total of 61 years from 1950 to 2010 are ranked based on the detrended number of intense U.S. tornadoes in AM. The top ten extreme U.S. tornado outbreak years are listed with ENSO phase in spring and TNI index in AM for each year. Strongly positive (i.e., the upper quartile) and negative (i.e., the lower quartile) TNI index values are in bold and italic, respectively.

Ranking	Year	ENSO phase in spring	TNI index (detrended)
1	1974	La Niña persists	**1.30 (1.48)**
2	1965	La Niña transitions to El Niño	**1.39 (1.54)**
3	1957	La Niña transitions to El Niño	**0.57 (0.69)**
4	1982	El Niño develops	*-1.11* (*-0.89*)
5	1973	El Niño transitions to La Niña	-0.42 (-0.24)
6	1999	La Niña persists	**0.47 (0.75)**
7	1983	El Niño decays	**1.86 (2.08)**
8	2003	El Niño decays	*-1.24* (*-0.94*)
9	2008	La Niña decays	**1.41 (1.73)**
10	1998	El Niño transitions to La Niña	**1.69 (1.97)**

Table 3. The total of 61 years from 1950 to 2010 are ranked based on the detrended number of intense U.S. tornadoes in AM. The bottom ten years are listed with ENSO phase in spring and TNI index in AM for each year. Strongly positive (i.e., the upper quartile) and negative (i.e., the lower quartile) TNI index values are in bold and italic, respectively.

Ranking	Year	ENSO phase in spring	TNI index (detrended)
52	1958	El Niño decays	-0.61 (-0.49)
53	1955	La Niña persists	-0.27 (-0.16)
54	2001	La Niña decays	0.21 (0.50)
55	1986	El Niño develops	-0.39 (-0.16)
56	1988	El Niño transitions to La Niña	-0.37 (-0.13)
57	1987	El Niño persists	0.10 (0.34)
58	1992	El Niño decays	0.21 (0.47)
59	1952	Neutral	-0.67 (-0.57)
60	1951	La Niña transitions to El Niño	-0.31 (-0.22)
61	1950	La Niña persists	**0.77 (0.86**)

Table 4. Prescribed SSTs in the tropical Pacific region for each model experiment. All model experiments are initiated from April of the prior year to December of the modeling year. For instance, in EXP_TNI, the model is integrated for 21 months starting in April using the composite April SSTs of 1956, 1964, 1973, 1998, and 2007.

Experiments	Prescribed SSTs in the tropical Pacific region
EXP_CLM	Climatological SSTs are prescribed in the tropical Pacific region (15°S–15°N; 120°E-coast of the Americas).
EXP_TNI	Composite SSTs of the five positive phase TNI years transiting from a La Niña identified among the ten most active U.S. tornado years (1957, 1965, 1974, 1999, and 2008) are prescribed in the tropical Pacific region.
EXP_TN1	Same as EXP_TNI except that the composite SSTs of the top ten positive TNI years are prescribed in the tropical Pacific region.
EXP_TN2	Same as EXP_TNI except that the composite SSTs of the top ten most extreme tornado years are prescribed in the tropical Pacific region.
EXP_LAN	Composite SSTs of the four years with a La Niña transitioning (1950, 1951, 1955 and 2001) identified among the ten least active U.S. tornado years are prescribed in the tropical Pacific region.
EXP_ELN	Composite SSTs of the four years with an El Niño transitioning (1958, 1987, 1988 and 1992) identified among the ten least active U.S. tornado years are prescribed in the tropical Pacific region
EXP_CPC	Same as EXP_TNI except that the composite SSTs are prescribed only in the western and central tropical Pacific region (15°S–15°N; 120°E - 110°W), while in the eastern Pacific region (15°S–15°N; 110°W-coast of the Americas) climatological SSTs are prescribed.
EXP_EPW	Same as EXP_TNI except that the composite SSTs are prescribed only in the eastern tropical Pacific region (15°S–15°N; 110°W-coast of the Americas), while in the western and central tropical Pacific region (15°S–15°N; 120°E - 110°W) climatological SSTs are prescribed.
EXP_011	SSTs for 2010-2011 are prescribed in the tropical Pacific region.
EXP_WPW	Same as EXP_011 except that the SSTs for 2010-2011 are prescribed only in the western Pacific region (15°S–15°N; 120°E - 180°).

Figure 1. The number of all (F0 – F5) U.S. tornadoes for the most active tornado months of April and May (AM) during 1950-2010 obtained from SWD.

Figure 2. (a) The number of intense (F3 – F5) U.S. tornadoes and (c) the intense tornado-days for the most active tornado months of April and May (AM) during 1950-2010 obtained from SWD. The intense U.S. tornado-days is obtained by counting the number of days in which more than three intense tornadoes occurred. The detrended number of intense tornadoes and the detrended intense tornado-days are shown in (b) and (d), respectively.

Figure 3. Scatter plot of the TNI (computed from ERSST3) versus the detrended number of intense U.S. tornadoes (obtained from SWD) in AM during 1950-2010. The green line shows the least-squares regression fit with its slope (α = 4.96) exceeding 99% confidence limit. The vertical lines to the left and right of the zero line show the lower and upper quartiles of the TNI index, respectively. The horizontal lines above and below the mean separate normal activity years from the 10 most active and 10 least active years.

Figure 4. Anomalous geopotential height and wind at 500 hPa, moisture transport and lower-level (850 – 1000 hPa) vertical wind shear for the ten most active U.S. tornado years (a, b and c) and the ten least active U.S. tornado years (d, e and f) in AM during 1950-2010 obtained from NCEP-NCAR reanalysis. The units are kg $m^{-1}sec^{-1}$ for moisture transport, m for geopotential height, and m s^{-1} for wind and wind shear. The small box in (a) - (f) indicates the central and eastern U.S. region frequently affected by intense tornadoes (30^{o}N-40^{o}N, and 100^{o}W-80^{o}W). The values of the 90% confidence interval averaged over the box region are 15 (17) and 0.5 (0.4) for b (e) and c (f), respectively.

Figure 5. Anomalous (a) geopotential height and wind at 500 hPa, (b) moisture transport and (c) lower-tropospheric (850 – 1000 hPa) vertical wind shear for the top ten positive TNI years in AM during 1950-2010 obtained from NCEP-NCAR reanalysis. The units are kg $m^{-1}sec^{-1}$ for moisture transport, m for geopotential height, and m s^{-1} for wind and wind shear. The small box in (a) - (c) indicates the central and eastern U.S. region frequently affected by intense tornadoes

(30^oN-40^oN, and 100^oW-80^oW). The values of the 90% confidence interval averaged over the box region are 16 and 0.5 for b and c, respectively.

Figure 6. Incidents of intense (F3-F5) U.S. tornadoes in AM for (a) the top ten positive TNI year, (b) ten neutral TNI years, and (c) the top ten negative TNI years during 1950-2010 obtained from SWD. Green color is for F3, blue color for F4 and red color for F5 tornadoes.

Figure 7. Composite SST anomalies in AM, obtained from ERSST3, for (a) the five positive TNI years transitioning from a La Niña identified among the ten most active U.S. tornado years in AM during 1950-2010, and for (b) the top ten positive TNI years and (c) the ten most active U.S. tornado years in AM during 1950-2010. Thick black rectangles indicate the Niño-4 (5°N - 5°S; 160°E - 150°W) and Niño-1+2 (10S° - 0°; 90°W - 80°W) regions. The values of the 90% confidence interval averaged over the tropical Pacific (15^oS-15^oN, and 120^oE-coast of the Americas) are 0.4, 0.3 and 0.3 for a, b and c, respectively.

Figure 8. Composite SST anomalies in AM, obtained from ERSST3, for (a) the four years with a La Niña transitioning and (b) the four years with an El Niño transitioning identified among the ten least active U.S. tornado years in AM during 1950-2010. The values of the 90% confidence interval averaged over the tropical Pacific (15^oS-15^oN, and 120^oE-coast of the Americas) are 0.4 and 0.5 for a and b, respectively.

Figure 9. Simulated anomalous (a) geopotential height and wind at 500 hPa, (b) moisture transport and (c) lower-level (850 – 1000 hPa) vertical wind shear in AM obtained from EXP_TNI – EXP_CLM. The units are kg m^{-1} sec^{-1} for moisture transport, m for geopotential height, and m s^{-1} for wind and wind shear. Thick black lines in (a) indicate the tropical Pacific region where the model SSTs are prescribed. The small box in (b) and (c) indicates the central and eastern U.S. region frequently affected by intense tornadoes (30^oN-40^oN, and 100^oW-80^oW). The values of the 90% confidence interval averaged over the box region are 17 and 0.5 for b and c, respectively.

Figure 10. Simulated anomalous geopotential height and wind at 500, moisture transport and (c) lower-level (850 – 1000 hPa) vertical wind shear in AM obtained from EXP_TN1 – EXP_CLM (a, b and c) and EXP_TN2 – EXP_CLM (d, e and f). The unit is kg m^{-1} sec^{-1} for moisture transport, m for geopotential height, and m s^{-1} for wind and wind shear. Thick black lines in (a) and (d) indicate the tropical Pacific region where the model SSTs are prescribed. The small box in (b), (c), (e) and (f) indicates the central and eastern U.S. region frequently affected by intense tornadoes (30^oN-40^oN, and 100^oW-80^oW). The values of the 90% confidence interval averaged over the box region are 23 (26) and 0.4 (0.6) for b (e) and c (f), respectively.

Figure 11. Same as Figure 11, but for EXP_LAN – EXP_CLM (a, b and c) and EXP_ELN – EXP_CLM (d, e and f). The values of the 90% confidence interval averaged over the box region are 22 (23) and 0.6 (0.5) for b (e) and c (f), respectively.

Figure 12. Same as Figure 11, but for EXP_CPC – EXP_CLM (a, b and c), and EXP_EPW – EXP_CLM (d, e and f). The values of the 90% confidence interval averaged over the box region are 20 (17) and 0.5 (0.5) for b (e) and c (f), respectively.

Figure 13. Simulated anomalous convective precipitation rate in AM obtained from (a) EXP_TNI – EXP_CLM, (b) EXP_CPC – EXP_CLM, and (c) EXP_EPW – EXP_CLM. The unit is mm day^{-1}. Thick black lines in (a) - (c) indicate the tropical Pacific region where the model SSTs are prescribed. The values of the 90% confidence interval averaged over the tropical Pacific (15^oS-15^oN, and 120^oE-coast of the Americas) are 4.7, 5.2 and 5.1 for a, b and c, respectively.

Figure 14. Background (climatological) vertical wind shear between 200 and 850 hPa in AM obtained from (a) NCEP-NCAR reanalysis, and (b) EXP_CLM. The unit is m sec^{-1}.

Figure 15. Anomalous SSTs in AM of three historical U.S. tornado outbreak years, namely (a) 2011, (b) 1974 and (c) 1925, obtained from ERSST3. The unit is °C.

Figure 16. Same as Figure 4, but for AM of 2011 (a, b and c) and of 1974 (d, e and f).

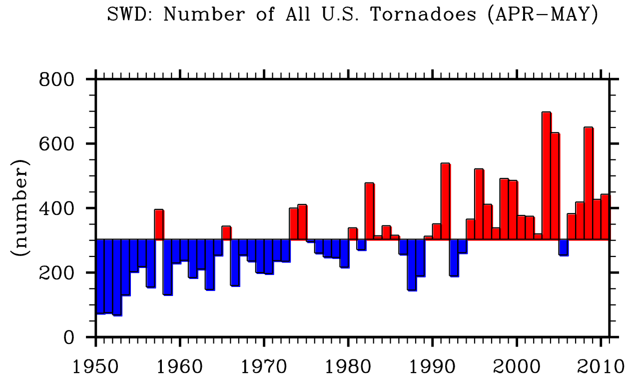

Figure 1. The number of all (F0 – F5) U.S. tornadoes for the most active tornado months of April and May (AM) during 1950-2010 obtained from SWD.

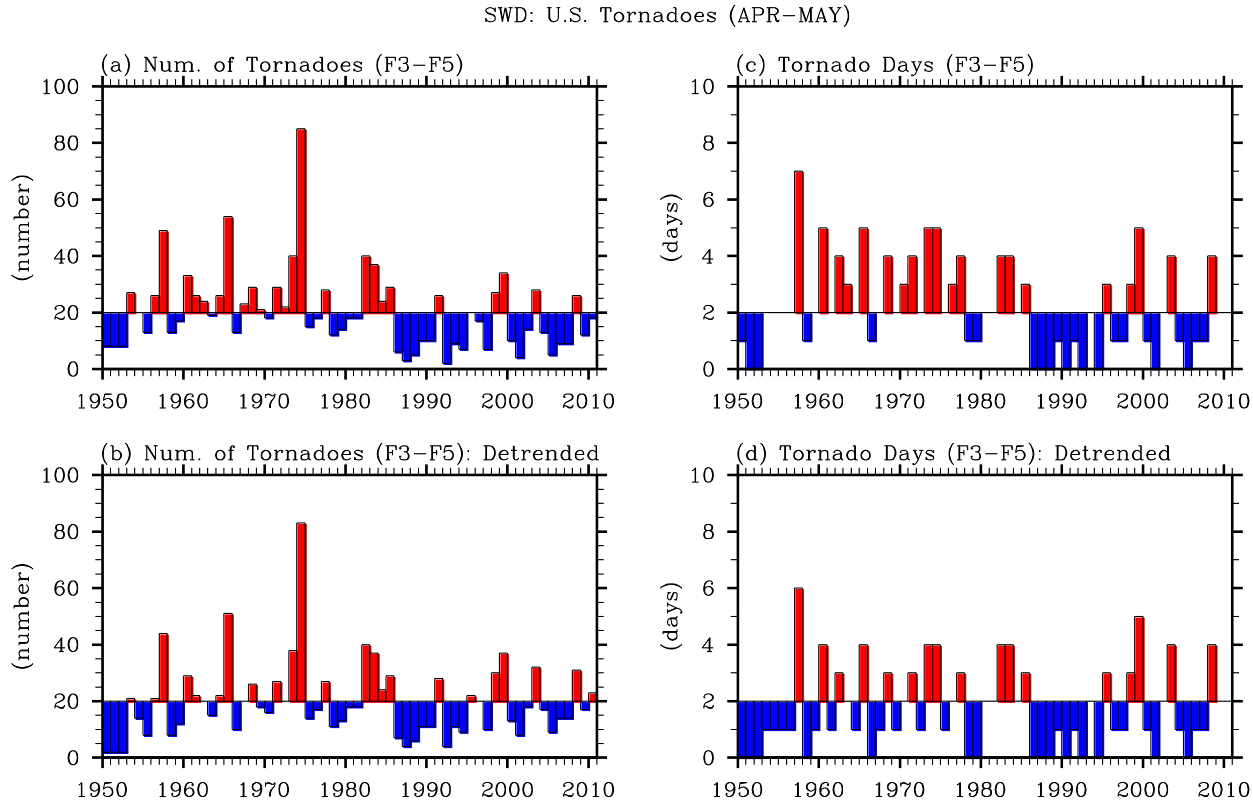

Figure 2. (a) The number of intense (F3 – F5) U.S. tornadoes and (c) the intense tornado-days for the most active tornado months of April and May (AM) during 1950-2010 obtained from SWD. The intense U.S. tornado-days is obtained by counting the number of days in which more than three intense tornadoes occurred. The detrended number of intense tornadoes and the detrended intense tornado-days are shown in (b) and (d), respectively.

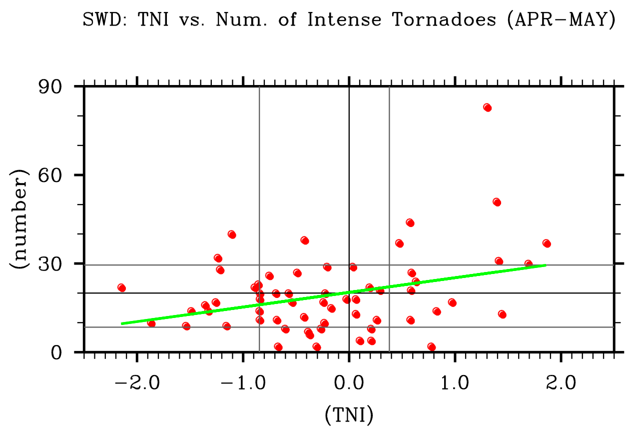

Figure 3. Scatter plot of the TNI (computed from ERSST3) versus the detrended number of intense U.S. tornadoes (obtained from SWD) in AM during 1950-2010. The green line shows the least-squares regression fit with its slope (α = 4.96) exceeding 99% confidence limit. The vertical lines to the left and right of the zero line show the lower and upper quartiles of the TNI index, respectively. The horizontal lines above and below the mean separate normal activity years from the 10 most active and 10 least active years.

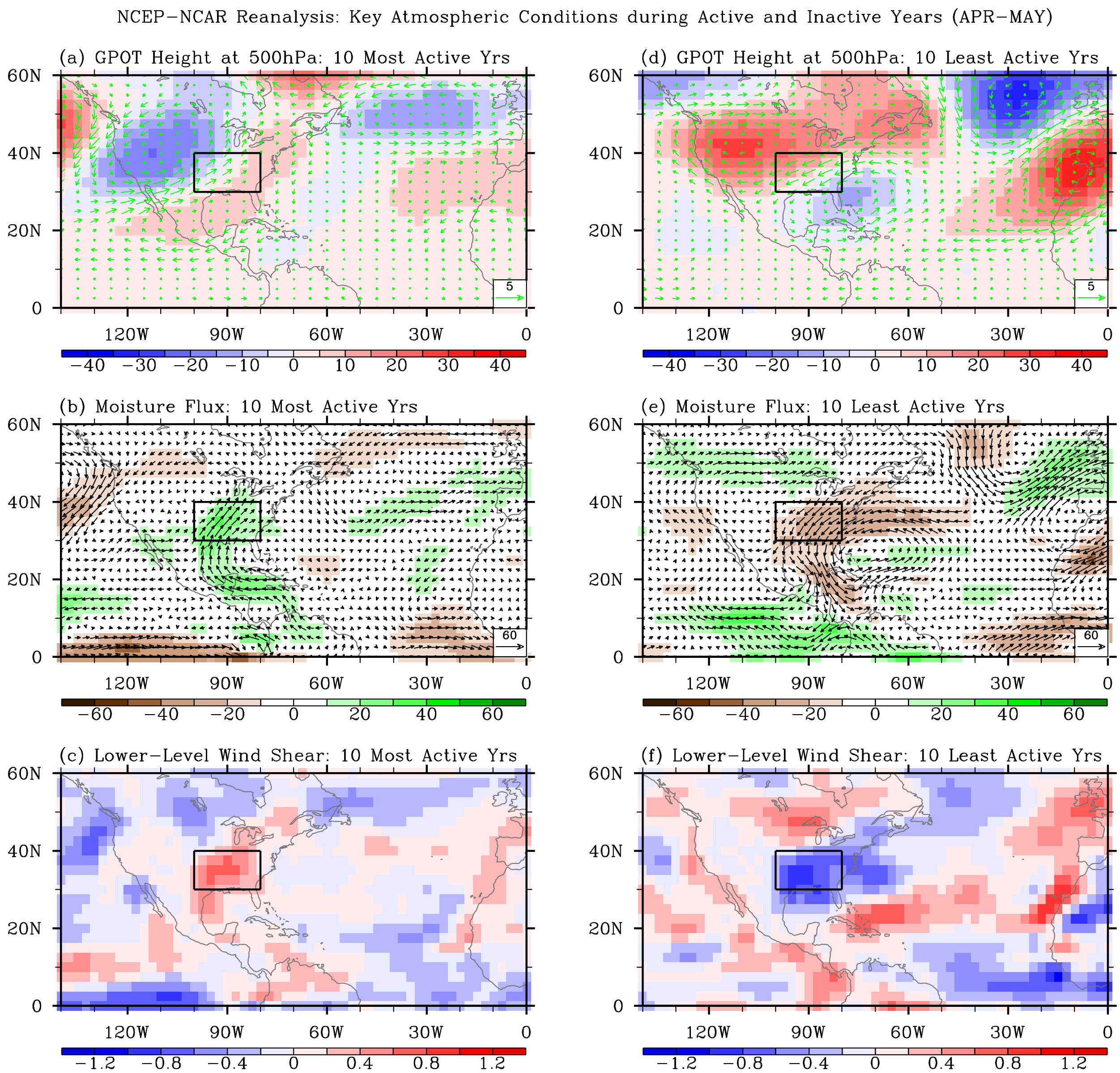

Figure 4. Anomalous geopotential height and wind at 500 hPa, moisture transport and lower-level (850 – 1000 hPa) vertical wind shear for the ten most active U.S. tornado years (a, b and c) and the ten least active U.S. tornado years (d, e and f) in AM during 1950-2010 obtained from NCEP-NCAR reanalysis. The units are kg $m^{-1}sec^{-1}$ for moisture transport, m for geopotential height, and m s^{-1} for wind and wind shear. The small box in (a) - (f) indicates the central and eastern U.S. region frequently affected by intense tornadoes (30^oN-40^oN, and 100^oW-80^oW). The values of the 90% confidence interval averaged over the box region are 15 (17) and 0.5 (0.4) for b (e) and c (f), respectively.

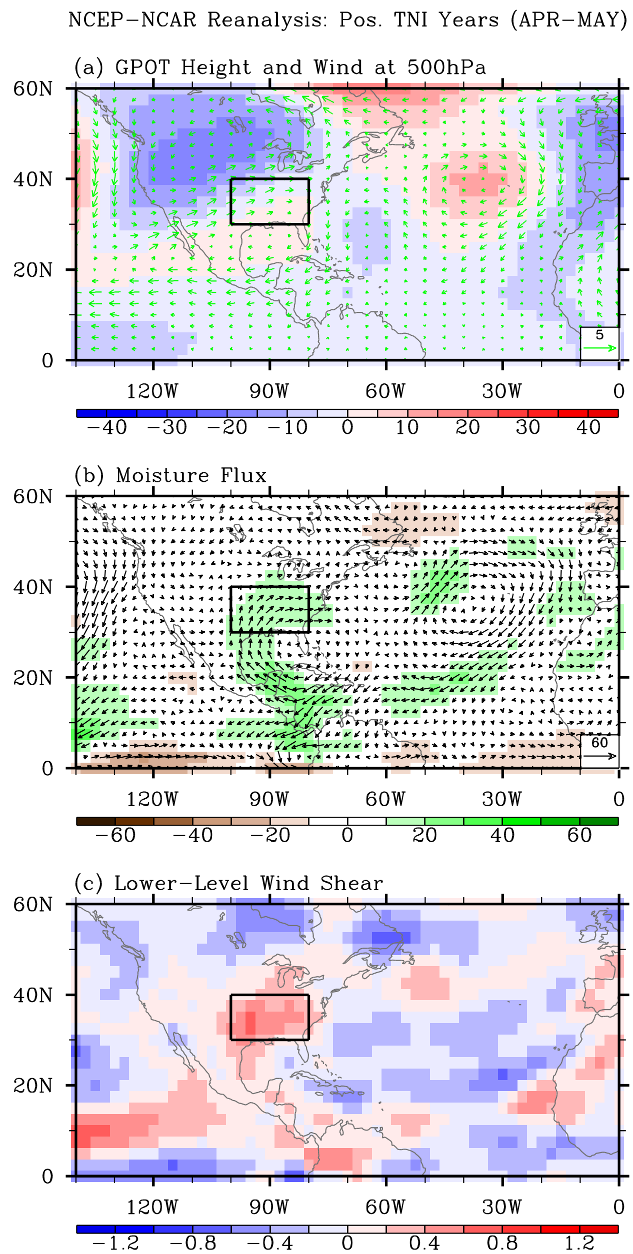

Figure 5. Anomalous (a) geopotential height and wind at 500 hPa, (b) moisture transport and (c) lower-tropospheric (850 – 1000 hPa) vertical wind shear for the top ten positive TNI years in AM during 1950-2010 obtained from NCEP-NCAR reanalysis. The units are kg $m^{-1}sec^{-1}$ for moisture transport, m for geopotential height, and m s^{-1} for wind and wind shear. The small box in (a) - (c) indicates the central and eastern U.S. region frequently affected by intense tornadoes (30^{o}N-40^{o}N, and 100^{o}W-80^{o}W). The values of the 90% confidence interval averaged over the box region are 16 and 0.5 for b and c, respectively.

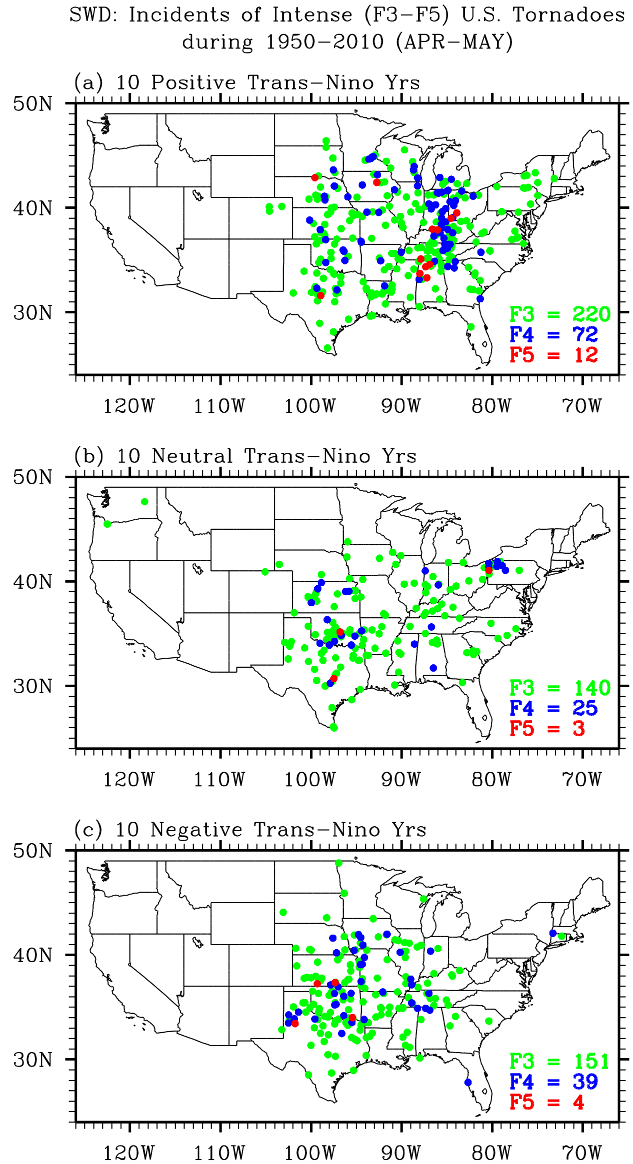

Figure 6. Incidents of intense (F3-F5) U.S. tornadoes in AM for (a) the top ten positive TNI year, (b) ten neutral TNI years, and (c) the top ten negative TNI years during 1950-2010 obtained from SWD. Green color is for F3, blue color for F4 and red color for F5 tornadoes.

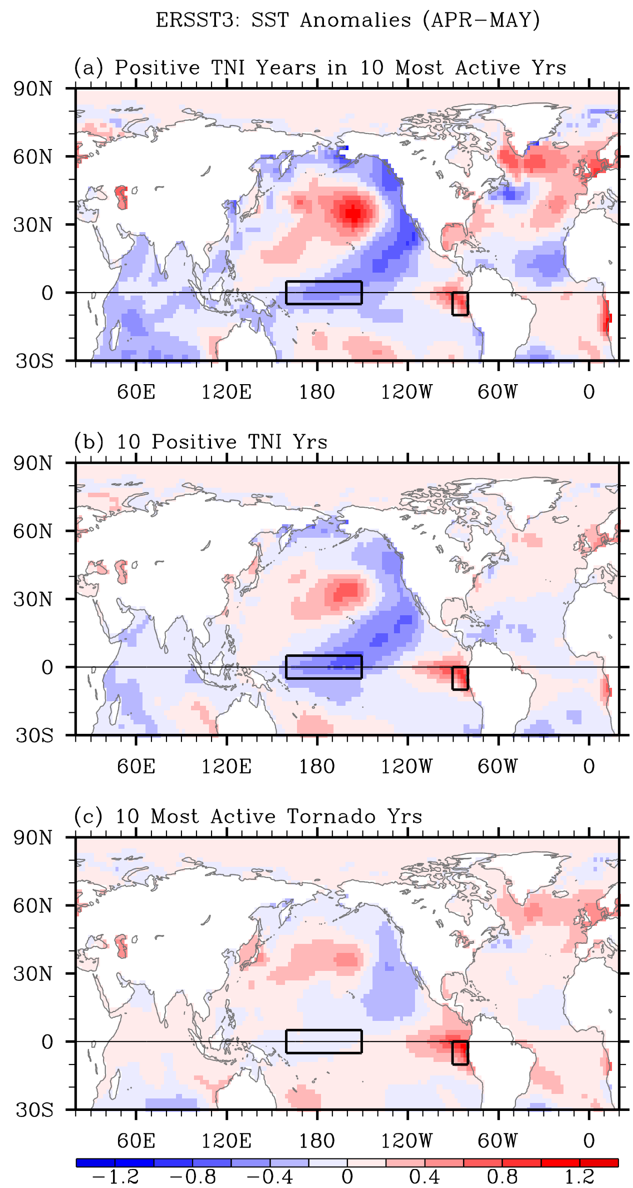

Figure 7. Composite SST anomalies in AM, obtained from ERSST3, for (a) the five positive TNI years transitioning from a La Niña identified among the ten most active U.S. tornado years in AM during 1950-2010, and for (b) the top ten positive TNI years and (c) the ten most active U.S. tornado years in AM during 1950-2010. Thick black rectangles indicate the Niño-4 (5°N - 5°S; 160°E - 150°W) and Niño-1+2 (10S° - 0°; 90°W - 80°W) regions. The values of the 90% confidence interval averaged over the tropical Pacific (15^{o}S-15^{o}N, and 120^{o}E-coast of the Americas) are 0.4, 0.3 and 0.3 for a, b and c, respectively.

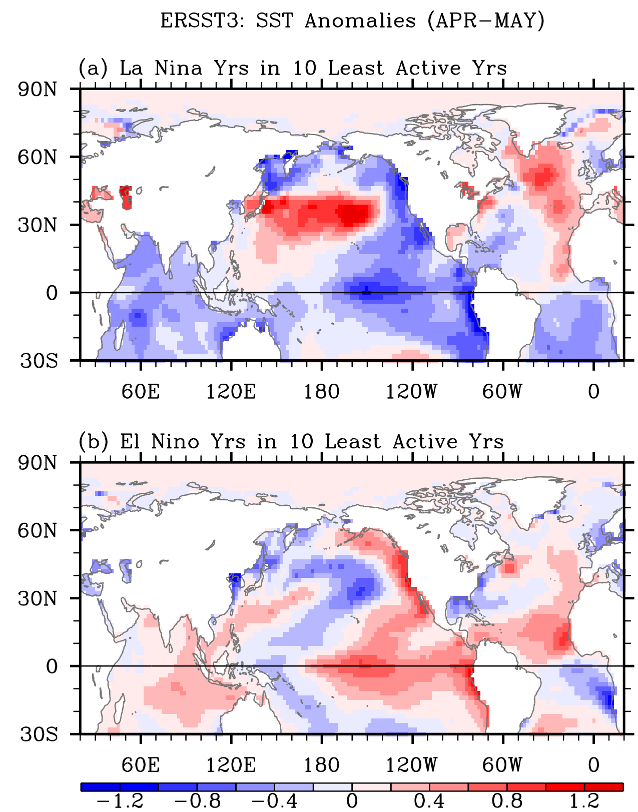

Figure 8. Composite SST anomalies in AM, obtained from ERSST3, for (a) the four years with a La Niña transitioning and (b) the four years with an El Niño transitioning identified among the ten least active U.S. tornado years in AM during 1950-2010. The values of the 90% confidence interval averaged over the tropical Pacific (15^{o}S-15^{o}N, and 120^{o}E-coast of the Americas) are 0.4 and 0.5 for a and b, respectively.

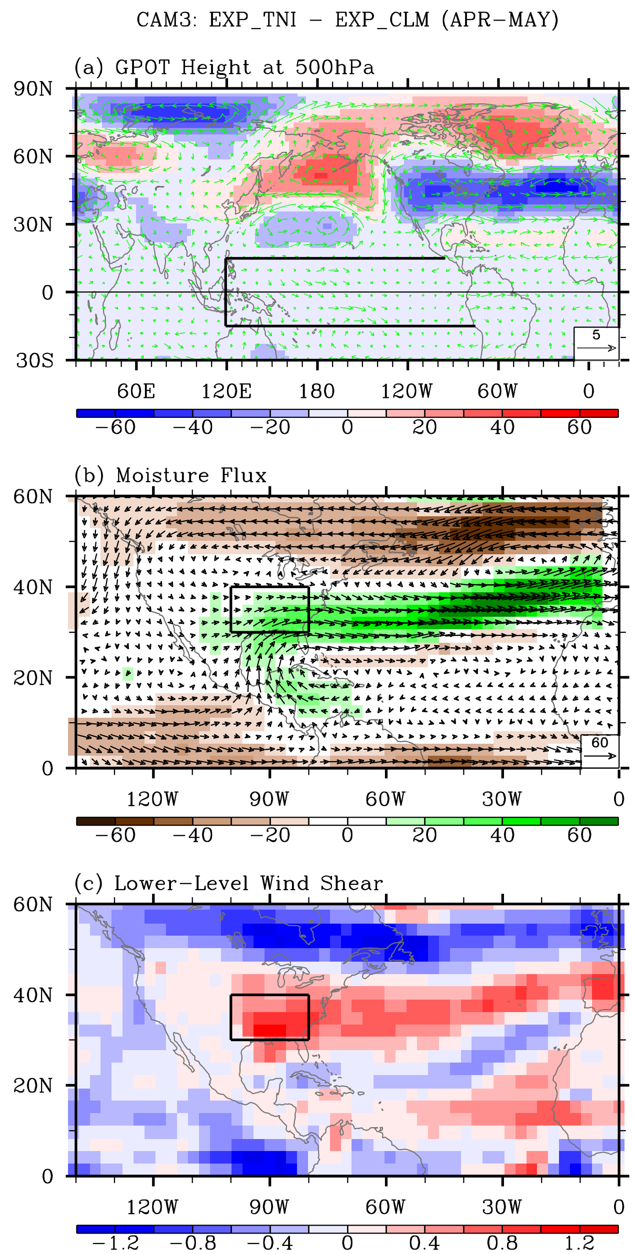

Figure 9. Simulated anomalous (a) geopotential height and wind at 500 hPa, (b) moisture transport and (c) lower-level (850 – 1000 hPa) vertical wind shear in AM obtained from EXP_TNI – EXP_CLM. The units are kg m^{-1} sec^{-1} for moisture transport, m for geopotential height, and m s^{-1} for wind and wind shear. Thick black lines in (a) indicate the tropical Pacific region where the model SSTs are prescribed. The small box in (b) and (c) indicates the central and eastern U.S. region frequently affected by intense tornadoes (30^{o}N-40^{o}N, and 100^{o}W-80^{o}W). The values of the 90% confidence interval averaged over the box region are 17 and 0.5 for b and c, respectively.

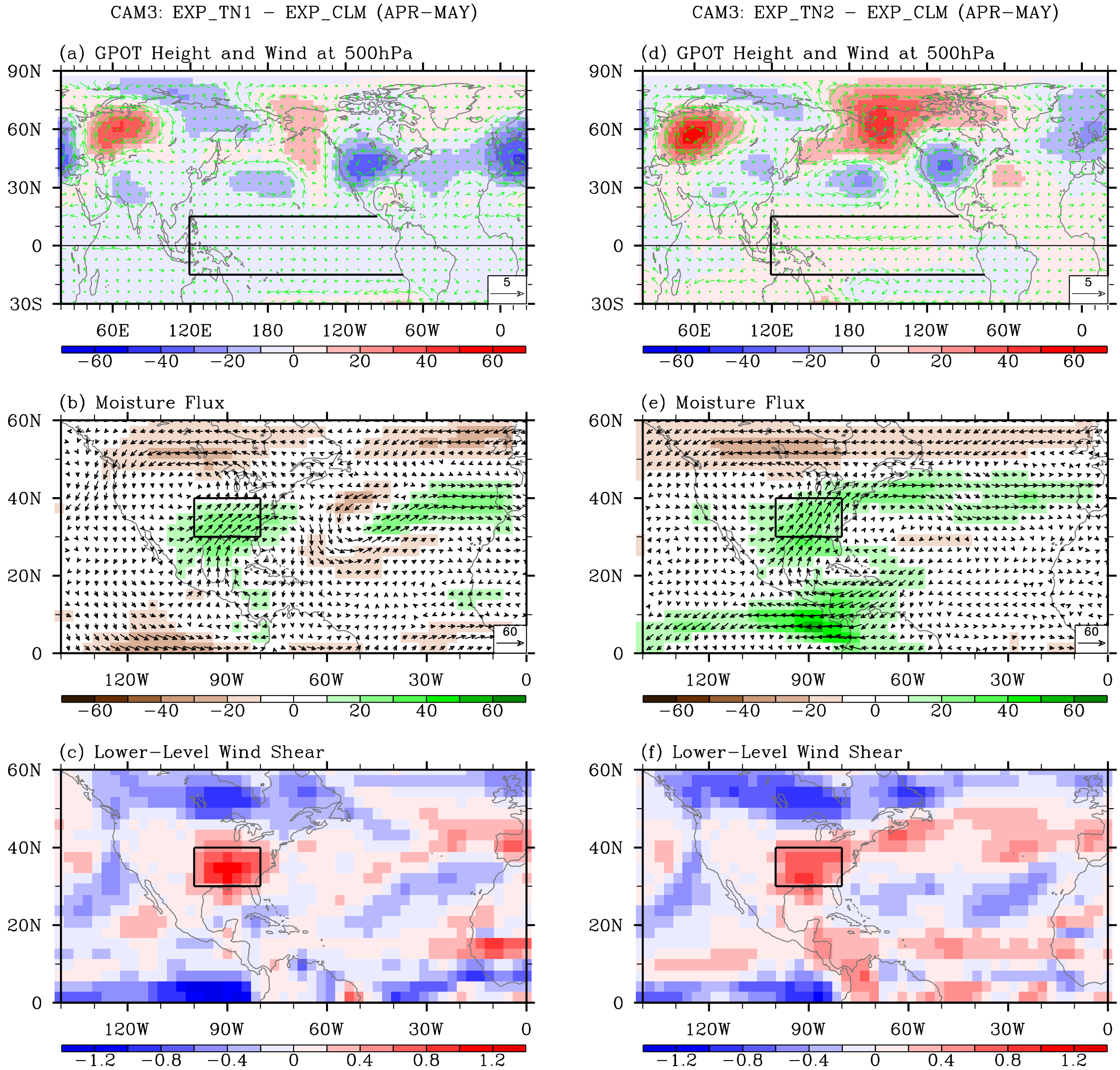

Figure 10. Simulated anomalous geopotential height and wind at 500, moisture transport and (c) lower-level (850 – 1000 hPa) vertical wind shear in AM obtained from EXP_TN1 – EXP_CLM (a, b and c) and EXP_TN2 – EXP_CLM (d, e and f). The unit is kg m^{-1} sec^{-1} for moisture transport, m for geopotential height, and m s^{-1} for wind and wind shear. Thick black lines in (a) and (d) indicate the tropical Pacific region where the model SSTs are prescribed. The small box in (b), (c), (e) and (f) indicates the central and eastern U.S. region frequently affected by intense tornadoes (30°N-40°N, and 100°W-80°W). The values of the 90% confidence interval averaged over the box region are 23 (26) and 0.4 (0.6) for b (e) and c (f), respectively.

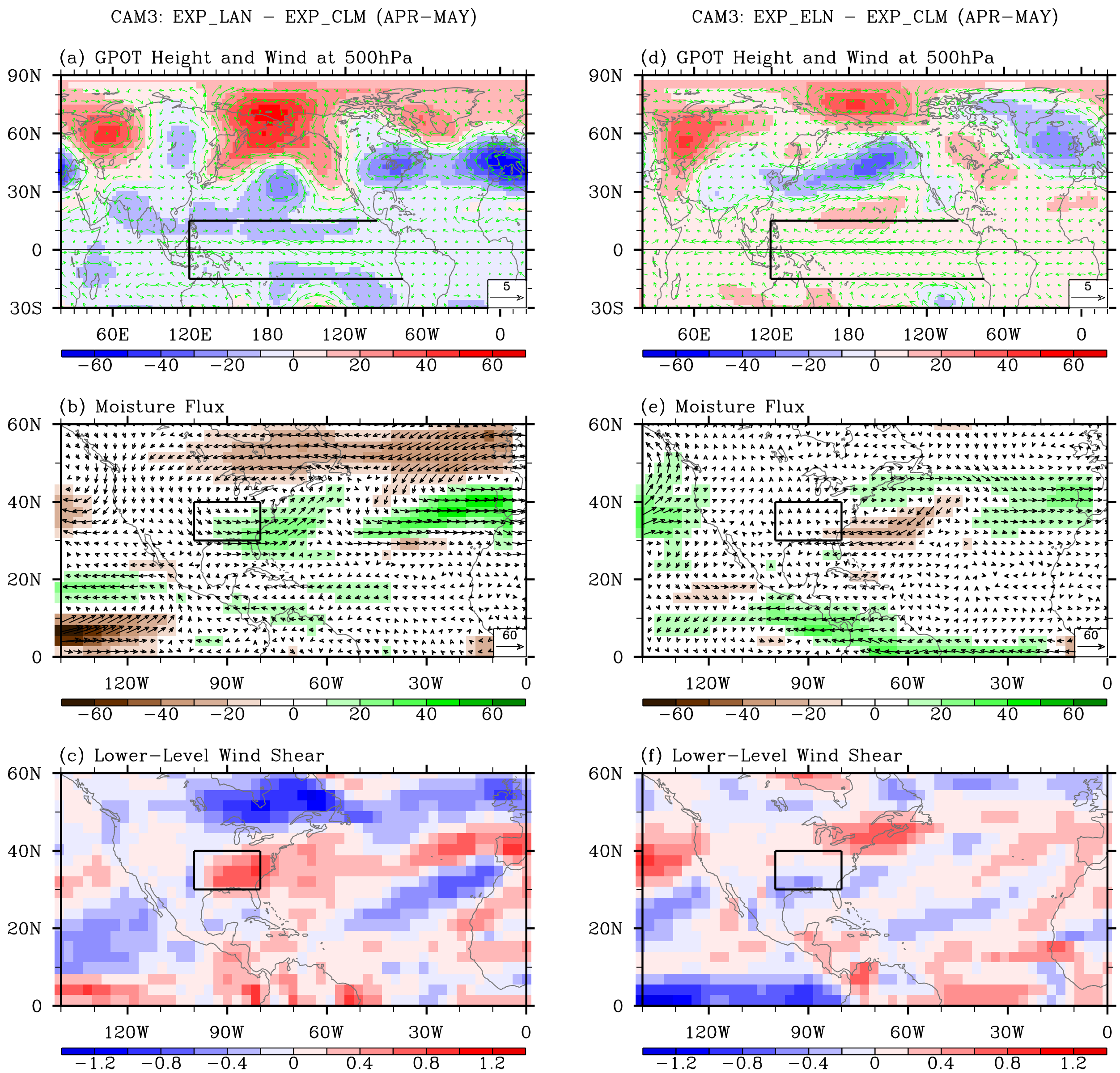

Figure 11. Same as Figure 11, but for EXP_LAN – EXP_CLM (a, b and c) and EXP_ELN – EXP_CLM (d, e and f). The values of the 90% confidence interval averaged over the box region are 22 (23) and 0.6 (0.5) for b (e) and c (f), respectively.

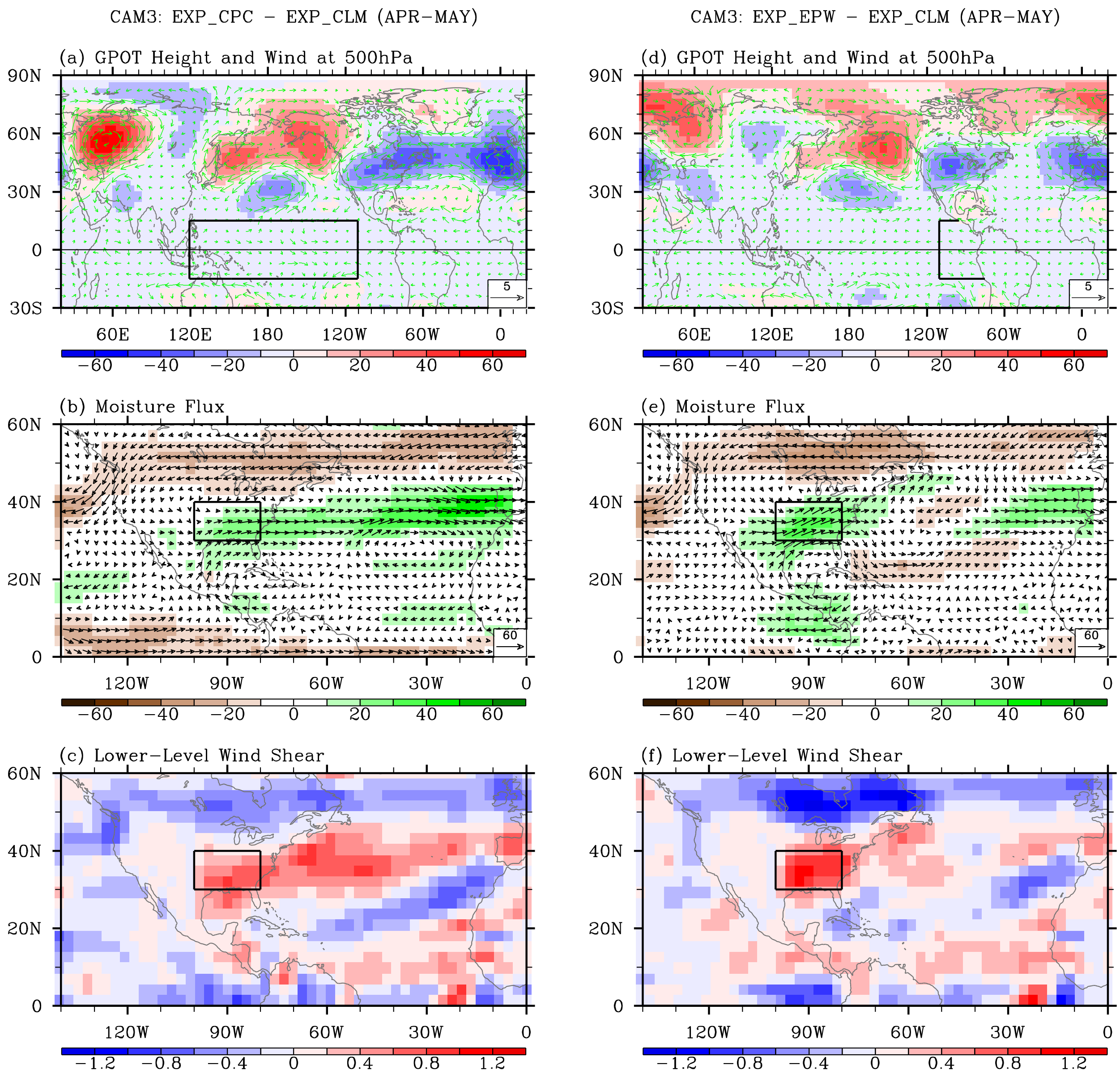

Figure 12. Same as Figure 11, but for EXP_CPC – EXP_CLM (a, b and c), and EXP_EPW – EXP_CLM (d, e and f). The values of the 90% confidence interval averaged over the box region are 20 (17) and 0.5 (0.5) for b (e) and c (f), respectively.

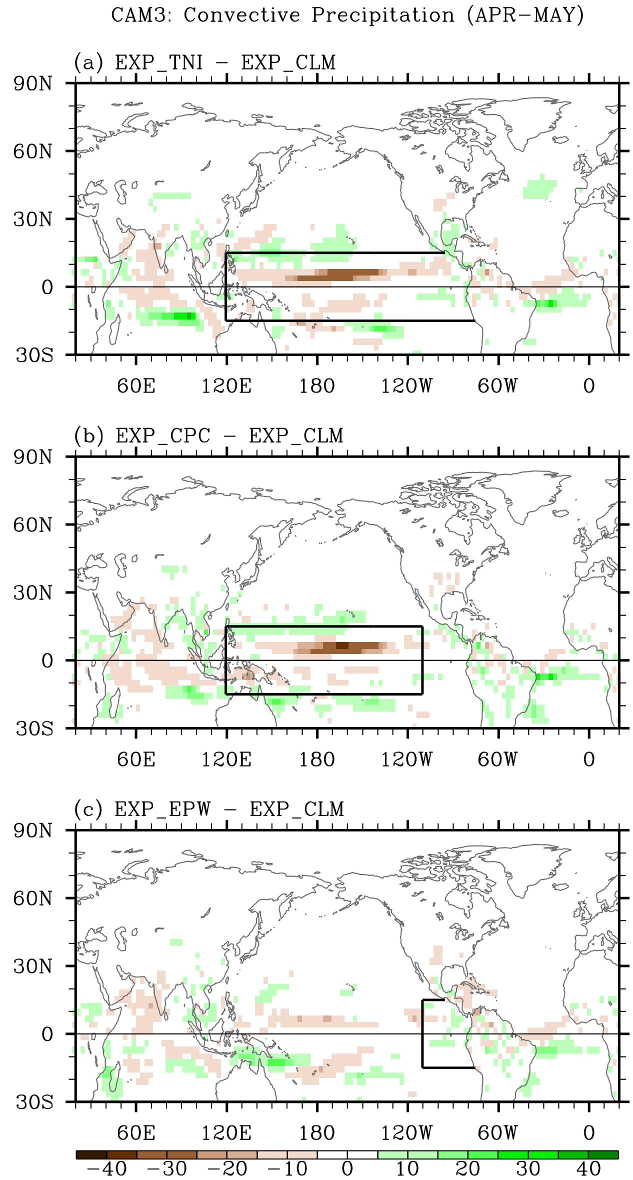

Figure 13. Simulated anomalous convective precipitation rate in AM obtained from (a) EXP_TNI – EXP_CLM, (b) EXP_CPC – EXP_CLM, and (c) EXP_EPW – EXP_CLM. The unit is mm day^{-1}. Thick black lines in (a) - (c) indicate the tropical Pacific region where the model SSTs are prescribed. The values of the 90% confidence interval averaged over the tropical Pacific (15^{o}S-15^{o}N, and 120^{o}E-coast of the Americas) are 4.7, 5.2 and 5.1 for a, b and c, respectively.

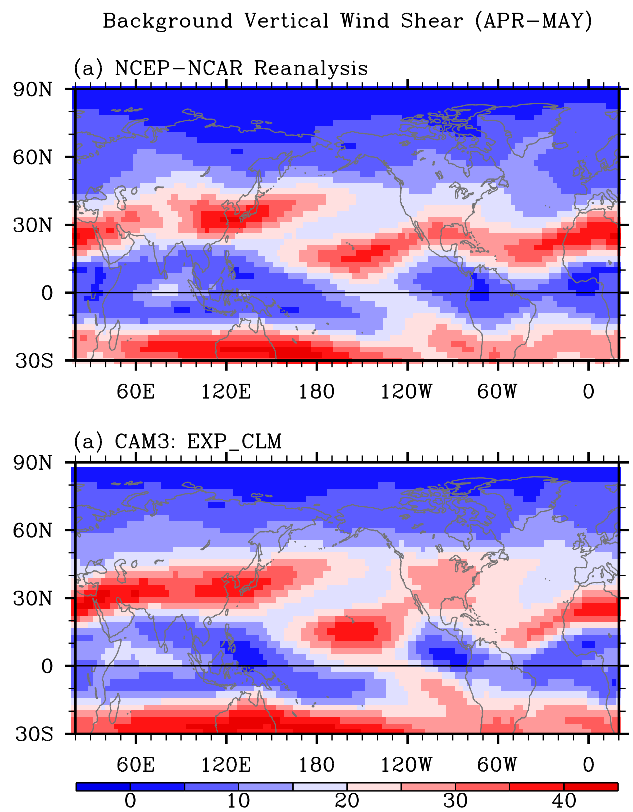

Figure 14. Background (climatological) vertical wind shear between 200 and 850 hPa in AM obtained from (a) NCEP-NCAR reanalysis, and (b) EXP_CLM. The unit is m sec $^{-1}$.

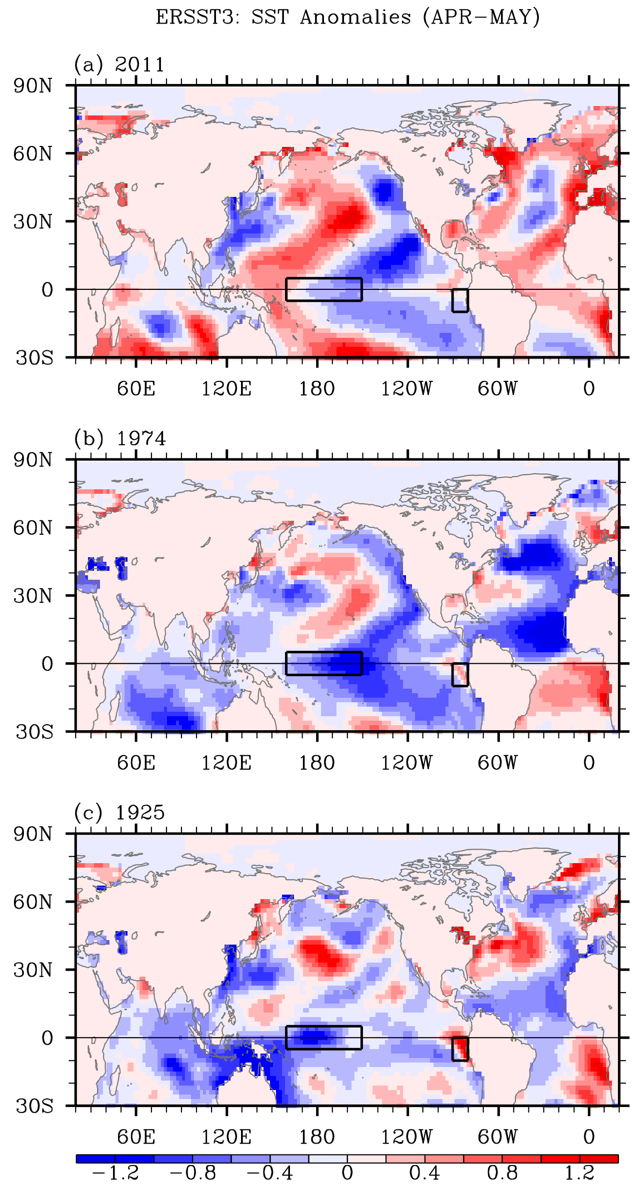

Figure 15. Anomalous SSTs in AM of three historical U.S. tornado outbreak years, namely (a) 2011, (b) 1974 and (c) 1925, obtained from ERSST3. The unit is °C.

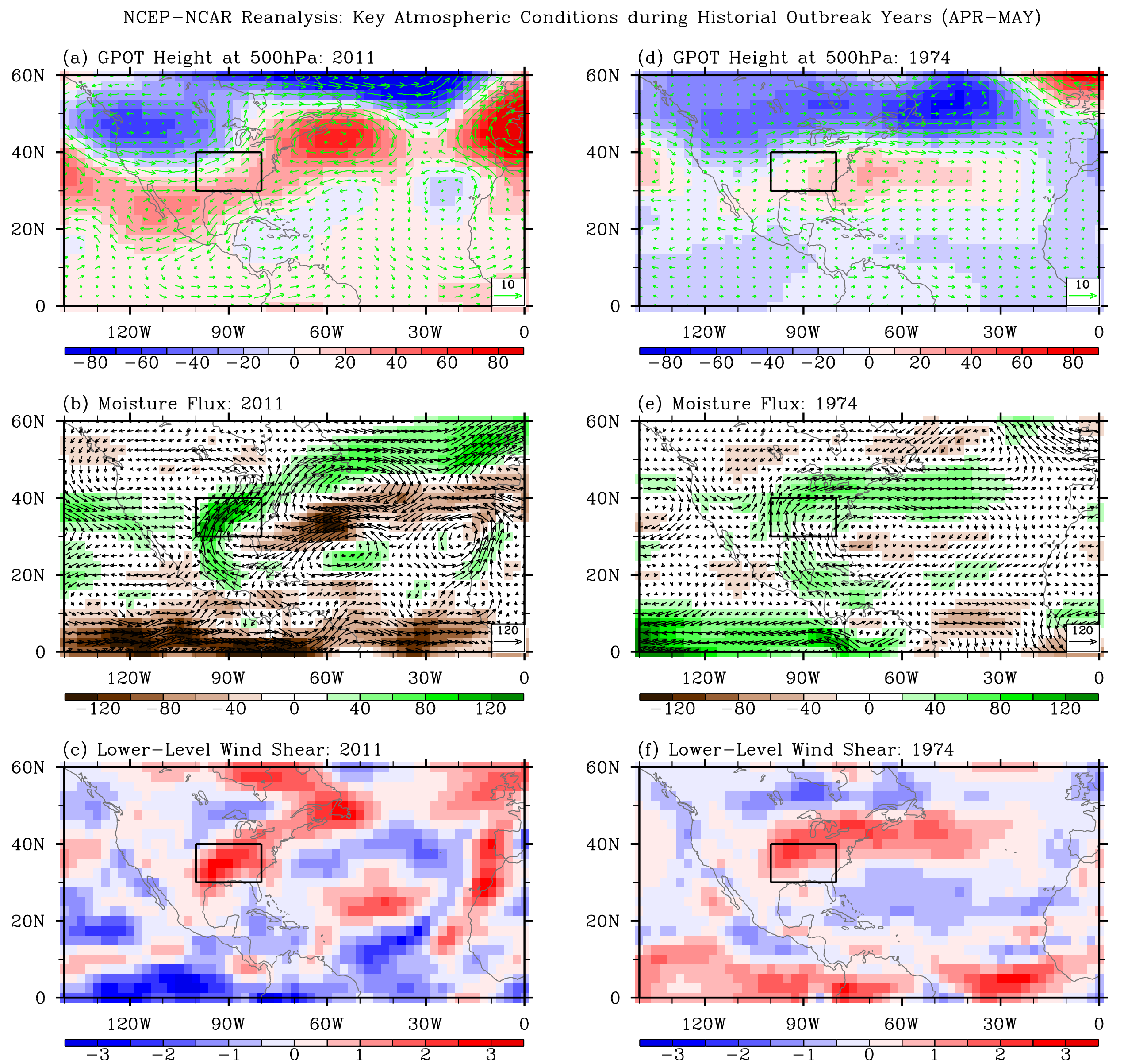

Figure 16. Same as Figure 4, but for AM of 2011 (a, b and c) and of 1974 (d, e and f).

Non-Rendered Figure 01
Click here to download Non-Rendered Figure: figure01.eps

Non-Rendered Figure 02

Click here to download Non-Rendered Figure: figure02.eps

Non-Rendered Figure 03
Click here to download Non-Rendered Figure: figure03.eps

Non-Rendered Figure 04

Click here to download Non-Rendered Figure: figure04.eps

Non-Rendered Figure 05
Click here to download Non-Rendered Figure: figure05.eps

Non-Rendered Figure 06
Click here to download Non-Rendered Figure: figure06.eps

Non-Rendered Figure 07
Click here to download Non-Rendered Figure: figure07.eps

Non-Rendered Figure 08

Click here to download Non-Rendered Figure: figure08.eps

Non-Rendered Figure 09
Click here to download Non-Rendered Figure: figure09.eps

Non-Rendered Figure 10
Click here to download Non-Rendered Figure: figure10.eps

Non-Rendered Figure 11

Click here to download Non-Rendered Figure: figure11.eps

Non-Rendered Figure 12

Click here to download Non-Rendered Figure: figure12.eps

Non-Rendered Figure 13
Click here to download Non-Rendered Figure: figure13.eps

Non-Rendered Figure 14
Click here to download Non-Rendered Figure: figure14.eps

Non-Rendered Figure 15

Click here to download Non-Rendered Figure: figure15.eps

Non-Rendered Figure 16
Click here to download Non-Rendered Figure: figure16.eps